Published in final edited form as:
Adv Drug Deliv Rev. 2014 September 30; 0: 2–20. doi:10.1016/j.addr.2014.07.011.

New Radiotracers for Imaging of Vascular Targets in Angiogenesis-related Diseases

Hao Hong[1,5], **Feng Chen**[1,5], **Yin Zhang**[2], and **Weibo Cai**[1,3,4]

[1]Department of Radiology, University of Wisconsin - Madison, WI, USA

[2]Department of Radiation Oncology and Molecular Radiation Sciences, Johns Hopkins University, MD, USA

[3]Department of Medical Physics, University of Wisconsin - Madison, WI, USA

[4]University of Wisconsin Carbone Cancer Center, Madison, WI, USA

Abstract

Tremendous advances over the last several decades in positron emission tomography (PET) and single photon emission computed tomography (SPECT) allow for targeted imaging of molecular and cellular events in the living systems. Angiogenesis, a multistep process regulated by the network of different angiogenic factors, has attracted world-wide interests, due to its pivotal role in the formation and progression of different diseases including cancer, cardiovascular diseases (CVD), and inflammation. In this review article, we will summarize the recent progress in PET or SPECT imaging of a wide variety of vascular targets in three major angiogenesis-related diseases: cancer, cardiovascular diseases, and inflammation. Faster drug development and patient stratification for a specific therapy will become possible with the facilitation of PET or SPECT imaging and it will be critical for the maximum benefit of patients.

Keywords

Angiogenesis; positron emission tomography (PET); single-photon emission computed tomography (SPECT); cancer; cardiovascular disease; inflammation

1. Introduction

Angiogenesis is critical for various growth and development relevant events including embryogenesis, tissue remodeling, and wound healing [1]. The sophisticated process is

Requests for reprints: Weibo Cai, PhD, Departments of Radiology and Medical Physics, School of Medicine and Public Health, University of Wisconsin - Madison, Room 7137, 1111 Highland Ave, Madison, WI 53705-2275, USA. Fax: 1-608-265-0614, Tel: 1-608-262-1749, wcai@uwhealth.org OR Hao Hong, PhD, Department of Radiology, School of Medicine and Public Health, University of Wisconsin - Madison, 1111 Highland Ave, Madison, WI 53705-2275, USA. Fax: 1-608-265-0614, Tel: 1-608-263-9566, hhong@uwhealth.org.
[5]Hao Hong and Feng Chen contributed equally to this work

usually regulated in a spatial and temporal manner via active interactions between angiogenic factors, extracellular matrix (ECM) components, and various types of cells. Imbalanced angiogenesis will lead to angiogenic disorders and destructive process of diseases, such as cardiovascular diseases (CVD, e.g. atherosclerosis), inflammation, and tumor growth/metastasis [2].

The pivotal process of angiogenesis can be divided into multiple stages. At the initial stage, the angiogenic stimuli activate the endothelial cells (ECs, the essential building blocks of all vessels) by enhancing their permeability and proliferation, resulting in new capillary sprout elongation [3]. The following stage involves the degradation of membrane matrix components to promote the invasion of ECs into the stroma from the proximal tissue [4], where matrix metalloproteinases (MMPs) are of critical importance. After the migration of ECs, the buildup of lumen is confirmed with the formation of multicellular vessel sprout. The final stage of angiogenesis is the stabilization of newly formed capillary. Disruption of angiogenesis is a critical factor of many pathological disorders, such as insufficient vascular density observed in myocardial or limb ischemia [5, 6] or irregular vascular growth and abnormal remodeling in primarily tumors [7] development.

In normal conditions, angiogenesis and inflammation are collaborators in the tissue repair and remodeling following tissue damage or destructive process of disease. In contrast, a detrimental relationship between angiogenesis and inflammation can result in diseases like asthma, atherosclerosis, diabetes, abdominal aortic aneurysm, inflammatory bowel diseases, and rheumatoid arthritis (RA) [8–12]. Acute inflammation usually triggers a protective defense against the “intruders”, which involves rapid recruitment and activation of various immune/inflammatory cells to fight against pathogens [13, 14]. On the other hand, chronic inflammation can cause substantial tissue damage which might facilitate carcinogenicity [15], where pathological angiogenesis (i.e. angiogenesis process under pathological states, e.g. tumorigenesis and inflammation) promotes a continuous recruitment of inflammatory cells, exacerbating inflammation and damage [16]. A number of inflammatory cells (e.g. neutrophils, eosinophils, mast cells, natural killer (NK) cells, macrophages, and dendritic cells (DCs)) are involved in inducing and promoting angiogenesis. Under hypoxia condition, these inflammatory cells can secrete a plethora of angiogenesis-boosting molecules, including vascular endothelial growth factor (VEGF), tumor necrosis factor-α (TNF-α), and various cytokines, resulting in enhanced vascular permeability and additional recruitment of immune cells. Multiple types of leukocytes and macrophages also involve in the proteolytic remodeling of the ECM by releasing different types of proteases (MMPs, cathepsins, plasminogen, urokinase etc.) to stimulate blood vessel formation. Activation of these inflammatory cells will also lead to the production of reactive oxygen species (ROS), important stimuli of angiogenesis.

The interactions between these constituents result in an intricate and heterogeneous complex of cells and matrix in the pathological angiogenesis. To explore the mechanisms of angiogenesis in molecular level and identify potential targets for disease therapy/prevention, precise knowledge about the role/network of these molecules (e.g. pro- or anti- angiogenic factors, vascular targets, etc.) inside the angiogenic cascades will be extremely beneficial.

With an aim to demonstrate the pros and cons of the different vascular targets (Scheme 1 and Table 1) in the diagnosis and therapy of various diseases, herein we will summarize newly developed radiotracers for positron emission tomography (PET) or single-photon emission computed tomography (SPECT) imaging of these vascular targets in three major angiogenesis-related diseases (i.e. cancer, cardiovascular diseases, and inflammation). Future research directions in the field of molecular imaging of angiogenesis will also be discussed.

2. Vascular targets of pathological angiogenesis

The vascular targets of pathological angiogenesis can be categorized into three major types: (1) targets on the ECs, (2) targets on non-ECs (i.e. monocytes, macrophages, and stem cells etc.), (3) ECM proteins and proteases [17]. Numerous studies have been performed to identify the roles in angiogenesis of various molecule families including VEGFs and their receptors (VEGFRs) [18, 19], Tie receptors [20], integrins [21], other growth factor receptors [22–24], as well as various cell adhesion molecules [25–27]. Some of these targets have been extensively investigated for pro- or anti- angiogenic therapies, whereas many others are emerging as new validated targets.

The therapeutic potentials offered by targeting these vascular targets fascinate researchers/clinicians [28, 29]. A series of clinical trials used different pro-angiogenic factors for therapeutic stimulation of angiogenesis but most of these trials did not show satisfactory outcomes [29]. Alternative strategies involved the usage of angiogenesis-related cell therapies or microRNAs [30], are actively pursued. In contrast, drugs blocking vessel growth have been successful demonstrating efficacy in several diseases, leading to the regulatory approval of significant amount of anti-angiogenic molecules. One good example is the approval of VEGF-targeting agents in both cancer and eye disease [31]. However, not all patients (especially cancer patients) can benefit from these agents due to different VEGF/VEGFR expression profile in patients. At the same time, the diseases can develop resistance and become refractory toward the VEGF/VEGFR inhibitors [32]. The same situation also applies to anti-angiogenic therapies against other vascular targets [33–35]. Conflicting results from the anti-angiogenic therapies in cancer treatment have raised concerns on whether anti-angiogenic treatment may trigger a selection to produce tumors with higher invasiveness and metastasis capability [36].

For anti-angiogenic therapy to pose a persistent impact on patient treatment and management, a comprehensive knowledge of the molecular events in the disease development and drug responses is important. To date, most of the mechanisms behind anti-angiogenic therapeutics as well as resistance to specific drugs remain unclear. In the last two decades, molecular imaging is gaining more popularity in collecting molecular information from the in vivo interactions/signal pathways to evaluate receptor expression profile and treatment efficacy in an early and accurate manner [37, 38]. With the definition of “visualization, characterization, and measurement of biological processes at the molecular and cellular levels in living systems” [37], molecular imaging can serve as a useful tool to further our understanding of molecular mechanisms behind angiogenesis and boost the efficacy of angiogenic therapies. A wide variety of imaging modalities have been employed

to study the molecular pathways of angiogenesis including ultrasound, computed tomography (CT), magnetic resonance imaging (MRI), near-infrared fluorescence (NIRF), bioluminescence, SPECT, and PET [39, 40]. The inherent strengths and weaknesses from each modality make synergistic multimodality imaging systems (e.g. SPECT/CT, PET/CT, and PET/MRI) increasingly attractive as these hybrid systems become more available world-wide. Among all the molecular imaging modalities, non-invasive nuclear imaging including SPECT and PET could offer enormous opportunities to elucidate these mechanisms and facilitate the personalized angiogenic therapy due to their high detection sensitivity, limitless penetration depth, and accurate target specificity [41].

3. PET or SPECT imaging of vascular targets in cancer

3.1 Molecular imaging modalities: PET vs SPECT

With the support of different radionuclides, SPECT and PET are molecular imaging techniques that enable expression profile evaluation of molecular targets within a living subject. Both techniques have deep signal penetration and demonstrate high sensitivity in imaging of molecular targets/processes, hence they have been routinely used in the clinic for more than a decade [42]. The spatial resolution of PET or SPECT is not as high as CT or MRI (which has sub-millimeter resolution) [43]. However, high contrast resolution and capability of providing functional information in the nano- or picomolar range make these two imaging modalities highly attractive.

SPECT is more established, less expensive, and more widely available than PET. Typically SPECT scanners employ collimators to define the angle of incidence of emitted gamma rays [44], resulting in a very low detection efficiency ($< 10^{-4}$). Frequently used radioisotopes in SPECT imaging include technetium ^{99m}Tc ($t_{1/2}$: 6.0 h), indium ^{111}In ($t_{1/2}$: 2.8 d), iodine ^{123}I ($t_{1/2}$: 13.2 h), and ^{131}I ($t_{1/2}$: 8.0 d). One of the major advantages of SPECT imaging is that it can be used for simultaneous imaging of different radionuclides via the energy identification of the gamma photons emitted from various radioisotopes [45], thereby enabling simultaneous visualization of parallel biological events, although such strategy is not frequently adopted.

Compared with SPECT, PET possesses certain superiority and gains increasing popularity in both the preclinical and clinical settings. Since its development in the 1970s [46], PET adopted different positron-emitting isotopes for imaging purposes, among which the most popular choices include carbon ^{11}C ($t_{1/2}$: 20 min), fluorine ^{18}F ($t_{1/2}$: 110 min), copper $^{61/64}$Cu ($t_{1/2}$: 3.3 h and 12.7 h), gallium $^{66/68}$Ga ($t_{1/2}$: 9.5 and 1.1 h), zirconium ^{89}Zr ($t_{1/2}$: 78.4 h), and iodine ^{124}I ($t_{1/2}$: 100.2 h). More recently, PET imaging with metal isotopes has gained more popularity with significant amount of efforts devoted to the development of new ligands with enhanced stability and improved pharmacokinetics [47]. It is worth to point out that long-lived PET isotopes (e.g. ^{64}Cu or ^{89}Zr) are desirable for long-term observation of vascular targets expression levels.

Cancer is a major public health problem world-wide. It causes approximately one in four deaths in the United States in 2014 [48], with an estimated number of 1,665,540 new cases in 2014. PET or SPECT imaging can offer unique opportunities for evaluating the processes

that regulate the formation, progression, and therapeutic intervention of pathological angiogenesis [17, 49], especially in cancer. In the following text of this review article, the current progress in PET or SPECT imaging of different vascular targets will be discussed in more details focusing on three diseases: cancer, cardiovascular diseases, and inflammation.

3.2 VEGF/VEGFR

The VEGF/VEGFR signaling pathway plays major role in both normal vasculature development and disease transformation [19, 50]. The VEGF family is composed of seven members with a common VEGF homology domain [18]. Among them, VEGF-A is a homodimeric, disulfide-bound glycoprotein existing in multiple isoforms, e.g. $VEGF_{121}$ and $VEGF_{165}$, which also differ in their biological characters. The angiogenic functions of VEGF are primarily achieved by interactions with two endothelium-specific receptor tyrosine kinases, VEGFR-1 (Flt-1/FLT-1) and VEGFR-2 (Flk-1/KDR) [51]. VEGFR-1 is critical for mediating physiologic and developmental angiogenesis while VEGFR-2 is primarily involved in the mitogenic, angiogenic, and permeability-changing activities caused by VEGF. Based on extensive studies on these molecules, it was confirmed that over-expressed VEGF/VEGFR is a validated therapeutic target for multiple abnormalities. Thus, VEGF-/VEGFR-targeted molecular imaging can be used for studying the efficacy of anti-angiogenic therapeutics, improving cancer patient management, and clarifying the complexity of VEGF/VEGFR signaling during cancer progression/intervention [52].

VEGF/VEGFR imaging can provide invaluable insights for cancer, cardiovascular diseases, or inflammation. Molecular imaging of VEGF/VEGFR has been reported in extensive reviews [39–41, 52–54], and will not be the main focus of current review. Three categories of PET or SPECT agents for imaging of VEGF/VEGFR will be briefly summarized here.

Radiolabeled isoforms of VEGF, including $VEGF_{121}$ [55–58], $VEGF_{165}$ [59, 60], or single chain VEGF (scVEGF) [61, 62], belong to the first category. Since VEGFs are comparatively small proteins, random radiolabeling of them usually significantly reduces or eliminates the receptor binding affinity. There are two strategies which can minimize this affinity loss: site-specific labeling (e.g. introduction of a cysteine tag to react with specific radiolabeling reagent) [61], and the insertion of a protective sequence (e.g. introduction of a poly-lysine sequence at non-receptor-binding region to minimize the disruption of a crucial lysine for binding) [57].

The second category involves radiolabeled antibody or antibody fragments [63–69]. To the best of our knowledge, only VEGF-targeted antibody or antibody fragments were studied for imaging. In 2004, a humanized monoclonal antibody (mAb) against VEGF-A, named bevacizumab, was approved by the US food and drug administration (FDA) for the treatment of metastatic colorectal cancer in combination with 5-fluorouracil [70]. Radiolabeled bevacizumab PET was demonstrated to be capable of detecting the VEGF-A expression levels [68, 69, 71]. However, the uptake of radiolabeled bevacizumab in primary tumors was relatively low. In one study, ^{89}Zr-labeled bevacizumab failed to detect the breast tumor with 10 mm diameter despite up-regulated VEGF-A expression [68]. Adopting radiolabeled bevacizumab for VEGF imaging initially faced skepticism due to the high mobility and fast break-down of VEGFs in vivo. Further investigation revealed that the

tumor uptake from radiolabeled bevacizumab was a result of its interaction with $VEGF_{165}$ and $VEGF_{189}$ isoforms on the cell surface and/or the ECM [72]. To date no strict correlation has been established between the tumor uptakes from the antibody and expression of VEGF-A. Radiolabeled ranibizumab (Fab fragment of bevacizumab) was used for monitoring VEGF expression level in anti-angiogenic treatment of cancer [73]. Rapid blood clearance of radiolabeled ranibizumab and VEGF-driven tissue uptake resulted in faster peak of lesion-to-background ratios that enable prompt follow-up compared with radiolabeled bevacizumab.

The third category is radiolabeled VEGFR inhibitors [74–76]. Radiolabeled protein inhibitor of VEGFR (e.g. aflibercept) [76] and several small-molecule tyrosine kinase inhibitors (TKIs) [74, 75, 77] were used in different studies to detect VEGF/VEGFR related angiogenic process. Compared with VEGF isoforms or antibody (and its fragments), most of the radiolabeled TKIs are more hydrophobic resulting in low tumor uptake and high non-specific uptake in normal tissues.

Imaging VEGF and VEGFR expressions are critical for accurate diagnosis and efficacy monitoring of a given angiogenic treatment. Despite the success of radiolabeled bevacizumab (or ranibizumab) in the detection of different diseases [68, 69, 78], more rigid correlation between lesion uptake and VEGF/VEGFR expression level should be established in the future to confirm the applicability of these radiotracers in monitoring therapeutic response. Meanwhile, chemical modification or library screening should be carried out in existing VEGFR inhibitors to improve their in vivo pharmacokinetics and receptor-targeting efficiency. The low synthesis cost and fast pharmacokinetics (which can lead to rapid peak of lesion-to-background ratio) of these inhibitors can make them potentially useful for PET or SPECT imaging of VEGF/VEGFR. Lastly, development of VEGFR type-specific imaging agents which possess minimal cross-reaction may also provide the researchers invaluable insights into the understanding of pathological angiogenesis. For instance, mutated-$VEGF_{121}$ ($VEGF_{DEE}$) which exhibited high specificity for VEGFR-2 may be promising for potential translation to clinical studies [79].

3.3 Integrins

Integrins are cell adhesion receptors possessing active interactions with a number of factors including ECM proteins, immunoglobulin, growth factors, cytokines, and multiple proteases. With the composition of noncovalently associated α- and β-subunits [80], twenty-four different heterodimers of integrin were identified from 18 α-subunits and 8 β-subunits [21]. Most integrins recognize their specific ECM proteins via the binding with small peptide motifs including Arg-Gly-Asp (RGD), Glu-Ile-Leu-Asp-Val (EILDV), and Arg-Glu-Asp-Val (REDV). Due to the critical role of integrins in angiogenesis, they serve as valuable targets for diagnosis/therapy of different diseases, not limited to cancer.

3.3.1 Integrin $\alpha_v\beta_3$—As an important player in angiogenesis, integrin $\alpha_v\beta_3$ is expressed on both tumor-surrounding ECs and certain tumor cells with minimal presence in normal tissues [81]. Over-expression of integrin $\alpha_v\beta_3$ is associated with aggressiveness and metastasis rate of multiple types of cancer as well as their responses to therapies [82]. As

well-accepted ligands for integrin $\alpha_v\beta_3$, RGD peptides were actively adopted for delivering anti-cancer drugs or contrast agents for cancer therapy or diagnosis. Due to the space limitation of this review and many existing comprehensive review articles in the literature by many research groups, we will not elaborate PET or SPECT imaging of integrin $\alpha_v\beta_3$ and the interested readers can refer to references [17, 39, 41, 52, 81] for detailed information.

3.3.2 Integrin $\alpha_4\beta_1$ (VLA-4)—Another class of integrins that have investigated for imaging applications is integrin β_1 clusters, also named the very late antigen (VLA) owing to their late appearance after activation. Integrin $\alpha_4\beta_1$, also known as CD29 or VLA-4, is a transmembrane cell adhesion heterodimer primarily present on lymphocyte, monocyte and eosinophil. Cumulative evidences also suggest that VLA-4 is a critical factor participating in tumor growth, angiogenesis, and metastasis [83], therefore it can be used as a promising target for diagnosis and therapy of lymphoid malignancies.

One compound named N-[[4-[[[(2-ethylphenyl)amino]carbonyl]amino]phenyl] acetyl]-N(epsilon)-6-[(2E)-1-oxo-3-(3-pyridinyl-2-propenyl)]-l-lysyl-l-2-aminohexanedioyl-(1-amino-1-cyclohexane)carboxamide (LLP2A) was extensively studied for PET or SPECT imaging of VLA-4. LLP2A is a peptidomimetic ligand with high affinity and specificity (IC_{50} = 2 pM) for VLA-4. Starting from 2009, LLP2A derivatives, such as DOTA-LLP2A (DOTA: 1,4,7,10-tetraazacyclododecane-1,4,7,10-tetraacetic acid), DOTA-LLP2A-PEG (PEG: polyethylene glycol), and CB-TE2A-LLP2A (CB-TE2A: 4,11-bis(carboxymethyl)-1,4,8,11-tetraazabicyclo[6.6.2]hexadecane) were designed, synthesized, and radiolabeled with ^{111}In or ^{64}Cu for whole-body autoradiography or small-animal PET in VLA-4 positive Raji B-cell lymphoma xenografts [84]. High tumor uptake was observed with radiolabeled DOTA-LLP2A and DOTA-LLP2A-PEG. Interestingly, tetravalent $(DOTA\text{-}LLP2A)_4$-PEG did not show higher tumor uptake than the monovalent DOTA-LLP2A or DOTA-LLP2A-PEG and led to higher liver, marrow, and kidney uptake instead. ^{64}Cu-CB-TE2A-LLP2A demonstrated obvious spleen uptake but little accumulation in kidney and liver (Figure 1a).

Subsequently, ^{64}Cu-CB-TE2A-LLP2A was used in another study to detect bone marrow-derived (BMD) cells which serves as an indicator of “premetastatic niche” formation before the metastatic cascade [85]. Binding validation of ^{64}Cu-CB-TE2A-LLP2A to VLA-4 was carried out in human melanoma B16F10 (VLA-4^+) and triple-negative breast cancer MDA-MB-231 (VLA-4^-). High uptake of ^{64}Cu-CB-TE2A-LLP2A was observed in the VLA-4-rich organs (e.g. the marrow, spleen, and the VLA-4-positive tumors). In nude mice implanted with firefly luciferase transfected MDA-MB-231, an induction of VLA-4-positive BMD cells was observed in the leg bone of mouse and corresponded to metastasis. Histological and flow cytometric analysis confirmed the up-regulation of VLA-4-positive cell populations (i.e. BMD cells) in the metastatic spots. Imaging of BMD is typically challenging due to the presence of adjunct α_4-positive normal bone marrow cells, which accounted for the background uptake of ^{64}Cu-CB-TE2A-LLP2A. This study provided important information for non-invasive imaging of potential cancer metastasis origin.

To boost the VLA-4 targeting efficacy of LLP2A and optimize its in vivo kinetics, a cross-bridged macrocyclic compound with a methane phosphonic acid pendant arm (named CB-

TE1A1P) was conjugated to LLP2A [86]. CB-TE1A1P-LLP2A can react with ^{64}Cu under mild conditions to produce stable radiolabeled compound with high specific activity, while high temperature is required for efficient radiolabeling using CB-TE2A. The resulting ^{64}Cu-CB-TE1A1P-LLP2A gave over three-fold enhancement in tumor uptake, less renal retention, and higher tumor-to-blood and tumor-to-muscle ratios when compared to ^{64}Cu-CB-TE2A-LLP2A. ^{64}Cu-CB-TE1A1P-LLP2A also possessed improved detection efficiency of VLA-4 from the pre-metastatic niche. The same compound was used to detect and stage multiple myeloma (MM) in another study [87]. The over-expression of VLA-4 on MM cells is among the critical events during their adhesion to the bone marrow which incurs MM cell trafficking and their drug resistance. VLA-4 specificity of ^{64}Cu-CB-TE1A1P-LLP2A was validated in a VLA-4-positive 5TGM1 and other the VLA-4 rich organs. Blocking study was also successfully carried out to confirm VLA-4 specificity of ^{64}Cu-CB-TE1A1P-LLP2A.

A wide array of imaging techniques have been used to explore the function and regulation of integrins [88, 89]. Among all the imaging agents, many RGD-based PET or SPECT agents have entered clinical investigation [89, 90]. The promising results to date have established integrins as important targets for disease diagnosis, drug delivery and therapeutic interventions. For the integrin-targeted imaging agents, it is important to carefully tune their pharmacokinetics, toxicity, and lesion specificity/selectivity in preclinical models and translational studies before future regulatory approval can be achieved.

3.4 CD105

CD105 (also known as endoglin) is considered as one of the most reliable markers for EC proliferation, and it is over-expressed on most of tumor neovasculature [91, 92]. CD105 is a disulphide-linked homodimeric transmembrane protein (MW: 180 kDa). Cellular and tissue distribution of CD105 demonstrated its profound roles in angiogenesis, vascular development, and homeostasis [93]. CD105 is a critical protein in the development of cardiovascular system due to its exclusive expression on vascular endothelia of human embryos at 4–8 weeks post-pregnancy, with the transient up-regulation during heart septation and heart valve formation. A disrupted expression pattern of CD105 was reported to result in human fetuses with cardiac defects [93].

The biological functions of CD105 are usually achieved via the interaction with the transforming growth factor-β (TGF-β) receptor complex, with the modulation by TGF-β [94]. Microvessel density (MVD) identification from CD105 and CD31 immunohistology can serve as an independent prognostic factor for patient survival in almost all solid tumor types, and it is a currently well-accepted standard procedure for quantifying tumor angiogenesis [95, 96]. The selective over-expression of CD105 on actively proliferating ECs is not observed in quiescent ECs [91, 93, 97]. In addition, its expression abundance (up to 3 million copies per cell) is significantly higher than most of other angiogenesis-related targets (e.g. VEGFR, less than 0.2 million copies per cell) [92, 98, 99]. The aforementioned facts establish CD105 as an optimal target for the imaging of tumor vasculature.

3.4.1 CD105-targeted antibodies—An anti-CD105 mAb, MAEND3, was used in immunohistological study more than a decade ago to reveal the distribution pattern of CD105 in melanoma, and the staining results were consistent with the binding studies of ^{125}I-labeled TGF-β1 in melanoma cells with varied expression levels of CD105 [100]. In vivo targeting of CD105 was further carried out in a subcutaneous MCF-7 human breast cancer model utilizing two ^{125}I-labeled anti-CD105 mAb (i.e. SN6f and SN6j) [101]. Significant tumor growth suppression was witnessed in a systemic therapy with both ^{125}I-SN6f and ^{125}I-SN6j, whereas ^{125}I-labeled isotype-matched control IgG did not exhibit any anti-tumor efficacy in the same study. This is a pioneer study in targeting CD105 for anti-angiogenic therapy, although later studies demonstrated that MCF-7 tumor cells themselves are CD105-negative (i.e. exclusive CD105 expression on the tumor vasculature) [102, 103].

The first SPECT imaging study of CD105 was carried out in a melanoma model [104]. ^{111}In-labeled anti-CD105 mAb MJ7/18 effectively homed to allografts of melanoma in C57BL/6 mice after intravenous administration. The tumor contrast based on autoradiography was modest and subsequent histological examination confirmed that the mAb was accumulated in the periphery of the tumor mass with highest vessel density. In contrast, background level of tumor uptake was observed in mice injected with ^{111}In-labeled control mAb. In another study, imaging was carried out in a spontaneous canine mammary carcinoma model using ^{125}I-labeled MAEND3 [105]. The results from this study confirmed that targeting of CD105 is a viable strategy for tumor imaging in different tumor histotypes. The ^{125}I-labeled MAEND3 successfully delineated mammary adenocarcinomas after intravenous injection. The tumor uptake of the mAb was rapid and prominent, without observable systemic side effects in animals up to 3 month after injection of the tracer. A few years after these preclinical studies, a ^{99m}Tc-labeled anti-CD105 mAb (E9) was used for perfusion in freshly excised kidneys from renal carcinoma patients [106]. Radioactivity distribution pattern consistent with the tumor locations (identified by both MRI and histology) was observed by immunoscintigraphy. The radioactivity uptake in tumors was more than 10 folds higher than the corresponding normal kidneys. Moreover, ^{99m}Tc-E9 demonstrated the capability of identifying tumors which were not discovered by MRI.

Starting from 2010, a CD105-targeted antibody named TRC105 (a human/murine chimeric IgG1 derived from the parent antibody SN6j [107]), with a very high avidity for human CD105 (K_D: 2 ng/mL), was used for PET imaging of CD105 in a variety of animal models. A Phase I open-label study was completed recently to assess the safety, pharmacokinetics, and anti-tumor efficacy in advanced solid tumor patients and multiple Phase II therapy trials are planned or underway [108].

To collect information on its pharmacokinetics and tumor targeting capacity, TRC105 was labeled with ^{64}Cu for PET imaging of CD105 in a murine breast cancer model [102]. ^{64}Cu-DOTA-TRC105 was initially used and systematic validations were performed to confirm its CD105 binding capacity and specificity. Flow cytometry and fluorescence microscopy analysis suggested similar affinity to CD105 between TRC105 and DOTA-TRC105. PET imaging demonstrated that the 4T1 tumor uptake of ^{64}Cu-DOTA-TRC105 was fast, prominent, persistent, and CD105-specific, resulting in excellent tumor contrast.

One of the controlling factors to influence the accuracy of PET imaging with radiometal-labeled mAb is that the tracer should maintain sufficient stability in biological system during the imaging period, since PET scanner detects the signal from radiometal rather than the mAb itself. With the initial success of ^{64}Cu-DOTA-TRC105, a number of strategies were taken to optimize the in vivo distribution pattern of radiolabeled TRC105. Another commercially available chelator, 1,4,7-triazacyclononane-1,4,7-triacetic acid (NOTA), was used in a follow-up study to modify TRC105 and the in vivo kinetics of ^{64}Cu-NOTA-TRC105 was compared with that of ^{64}Cu-DOTA-TRC105 [103]. PET imaging along with biodistribution studies validated the improved in vivo stability of ^{64}Cu-NOTA-TRC105 over ^{64}Cu-DOTA-TRC105, evidenced by significantly lower liver uptake but similar tumor targeting efficiency. The superiority of NOTA over DOTA was confirmed in this study for PET imaging with ^{64}Cu-labeled TRC105. Subsequently, ^{66}Ga was also used to label NOTA-TRC105 because of the generally recognized excellent stability of ^{66}Ga-NOTA compounds [109]. Owing to the improved stability, more prominent blood radioactivity level and comparable liver uptake than those from ^{64}Cu-DOTA-TRC105 were observed with the tumor uptake of ^{66}Ga-NOTA-TRC105 being similar to that of ^{64}Cu-DOTA-TRC105. Two major limitations of using ^{66}Ga is the comparatively higher positron energy (E_{max}: 4.15 MeV, leading to a longer positron range) than ^{64}Cu (E_{max}: 0.656 MeV), and it has spontaneous gammas. Both of the factors can affect the reconstruction and quantitation of PET images, resulting in lower spatial resolution [110].

Recently, zirconium-89 (^{89}Zr) has become a highly popular isotope for immunoPET, since the physical half-life matches well with the time required for antibodies to achieve optimal tumor-to-background ratio[111]. TRC105 was conjugated with desferrioxamine (Df, an extensively investigated chelator for ^{89}Zr), and subsequently labeled with ^{89}Zr for in vivo targeting of CD105 in the 4T1 tumor model (Figure 1b) [112]. Tumor uptake of ^{89}Zr-Df-TRC105 was higher than all normal organs starting from 24 h to 96 h post-injection (p.i.) monitored by PET. The encouraging results from this study provided the basis for using dual-labeled TRC105 (^{89}Zr-Df-TRC105-800CW, 800CW indicates a near-infrared fluorescent [NIRF] dye with emission peak at 800 nm) to detect both the subcutaneous tumors and breast cancer lung metastasis [113, 114]. This dual-labeled TRC105 can enable not only detection of primary tumor or small lung metastasis but also intraoperative guidance for tumor resection. Similar results were also observed with ^{64}Cu and 800CW dual-labeled TRC105 [109, 115].

One limitation of radiolabeled intact antibodies lies in their prolonged circulation time [116], hence it typically takes a couple of days after injection to reach optimal tumor-to-normal tissue ratio. To overcome this limitation, antibody fragment-based PET tracers are employed owing to their specific targeting and rapid blood clearance, allowing for future same day immunoPET imaging in clinical settings. The representative examples are Fab and F(ab′)$_2$ fragments, which are produced by enzymatic digestion of mAb using papain and pepsin, respectively. These fragments have comparable antigenic specificity as their parent antibody, with better tumor penetration and faster blood clearance due to their smaller sizes (ranging from ~50 kDa to ~100 kDa) than the parent antibody (typically ~150 kDa). The characteristics of ^{64}Cu-labeled TRC105-F(ab′)$_2$ and TRC105-Fab for PET imaging of CD105 were also investigated in the 4T1 cancer model [117, 118]. With the rapid blood

clearance and tumor uptake of radiolabeled $F(ab')_2$ or Fab, ^{61}Cu-labeling was also able to provide sufficient tumor contrast at early time points. ^{61}Cu has a higher β^+ branching ratio (60% vs. 17%) and shorter decay half-life (3.4 h vs. 12.7 h) than ^{64}Cu, which can bring higher PET signal and lower radiation dosimetry to normal organs. The use of $F(ab')_2$ or Fab fragment of TRC105 led to faster tumor accumulation (which peaked at as early as 3 h p.i.) than radiolabeled TRC105 (which often peaked at or after 24 h p.i.) without significant compromise of the absolute uptake of the tracer.

Tumor uptake values in all these abovementioned studies with TRC105 were relatively low (< 15 %ID/g) for immunoPET largely due to two reasons. First, CD105-targeted antibodies specifically recognize the tumor vasculature rather than the tumor cells. Significantly fewer tumor vascular ECs (usually < 10%) were present when compared with tumor cells (the usual targets of most antibodies). Second, the antibody affinity to murine CD105 is much lower than its affinity to human CD105. Taken together these two facts, the tumor uptake of ~15 %ID/g for radiolabeled TRC105 in rodent models is rather remarkable, and it is likely that radiolabeled TRC105 may perform much better in future clinical studies than what was observed in preclinical tumor models.

3.4.2 CD105-targeted nanomaterials—Nanotechnology has high potentials for early detection, accurate diagnosis, and personalized treatment of various diseases, especially cancer [119]. Different nanomaterials with various unique properties have been used as useful tools to study angiogenic events [41]. Due to the abundant expression of CD105 in multiple types of cancer and its easy access (i.e. immediately accessible after intravenous injection of nanomaterials), CD105-targeted nanomaterials do not need to go beyond the vasculature to reach the target hence won't be limited by extravasation, one of the major hurdles facing by nanomaterial-based tumor targeting in vivo. CD105-targeted nanomaterials are actively being studied and can be used for both imaging and drug delivery simultaneously.

Graphene-based nanomaterials have attracted tremendous interests as biomedical vectors due to their unique physical/chemical properties [120]. Recently, functionalized nanographene oxides (GOs) with good CD105-specificity were developed and evaluated as a nanoplatform for potential image-guided drug delivery [121, 122]. GO was covalently linked to TRC105 and NOTA, and the product NOTA-GO-TRC105 was labeled with either ^{64}Cu [121] or ^{66}Ga [122]. Radiolabeled GO conjugates demonstrated high tumor-targeting efficiency in vivo measured by serial PET imaging, which was confirmed with biodistribution/histological examinations. The enhanced uptake in 4T1 tumor was confirmed to be specific for CD105 on the neovasculature, which warranted future investigation of these GO conjugates for CD105-targeted drug delivery and/or photothermal therapy. To further promote their therapeutic performance, functionalized reduced graphene oxide (RGO) with superior photothermal absorbance [123] was adopted in a following study using similar conjugation strategy [124]. Similar tumor uptake was observed using ^{64}Cu-NOTA-RGO-TRC105 and ^{64}Cu-NOTA-GO-TRC105. These studies successfully demonstrated the strategies of CD105-targeted delivery of grapheme nanomaterials which will be promising theranostic agents for both imaging and therapeutic purposes.

Other nanoplatforms used for CD105-targeting and imaging include unimolecular micelles [125, 126] and mesoporous silica nanoparticles [127]. In two parallel studies, unimolecular micelles were produced from dendritic amphiphilic block copolymers poly(amidoamine)-poly(L-lactide)-b-poly(ethylene glycol) [125] or poly(2-hydroxyethyl methacrylate) (PHEMA)-poly(l-lactide)-poly(ethylene glycol) [126] chemically modified with TRC105 and NOTA. Doxorubicin (DOX) was loaded into the hydrophobic core of these unimolecular micelles via physical encapsulation. After ^{64}Cu labeling, TRC105-conjugated micelles exhibited much higher tumor uptake when compared to non-targeted micelles, confirmed by PET imaging. With synergistically integrated passive and active tumor-targeting capacities, these theranostic unimolecular micelles demonstrated pH-controllable drug release and PET imaging capabilities. By using a similar conjugation scheme, CD105-targeted mesoporous silica nanoparticles (MSN) were generated [127]. Increased tumor uptake of MSN and enhanced delivery of DOX to tumor were observed in 4T1 tumor-bearing mice revealed by PET and fluorescence imaging, respectively, indicating their high potentials for image-guided drug delivery for cancer therapy.

All the above-mentioned findings suggest that CD105-targeted PET or SPECT imaging of solid malignancies is a promising, safe, and universally applicable procedure [128]. Even though variable levels of CD105 expression can be found on the microvasculature of normal tissues, which is likely orders of magnitude lower than those on actively proliferating ECs [92, 97], the previously achieved encouraging results established the critical role of CD105 in cancer diagnosis and treatment.

3.5 MMPs

MMPs are a cluster of peptidases that can promote the degradation of the ECM [4]. ECM remodeling by MMPs is important in various physiological and pathological scenarios, ranging from organ formation/regeneration, angiogenesis, or inflammation, to tumor progression [3, 129–131]. Dysregulation of MMP activity can lead to different diseases including atherosclerosis, inflammation, and cancer [132].

Non-invasive PET or SPECT imaging of MMP activity in vivo can be achieved by either radiolabeled synthetic inhibitors or MMP-specific peptides [133, 134], which allows the characterization of atherosclerotic plaques, inflammatory lesions or tumors. An overview of radiolabeled MMP inhibitors (MMPIs) or MMP peptides for PET OR SPECT imaging of proteolytic activity of MMPs can be found in references [132–134]. Currently, PET or SPECT imaging of MMPs is still at a preliminary stage and no related clinical study has been reported yet. Compared with blooming studies in fluorescence imaging of MMPs [135], PET or SPECT imaging of MMPs enabled the researchers to observe the MMP distribution or activation in deeper tissues, but usually resulted in lower target-to-background ratio. In order to improve the PET or SPECT tracers for imaging of MMP, chemical modification of existing MMPIs to decrease the non-specific binding or using anti-MMP antibodies could be alternative strategies.

3.6 Tenascin-C (TNC)

TNC is a hexameric extracellular glycoprotein expressed upon tissue injury specifically and transiently [136, 137]. Four distinct domains constitute TNC which include an assembly domain, epidermal growth factor-like motifs, fibronectin III-like repeats, and a fibrinogen-resembled structure [137]. Among the tenascin family, the expression pattern of TNC is unique. TNC is undetectable in healthy adult tissues while many studies confirmed a vital role of TNC in cardiac and arterial injury, tumor angiogenesis/metastasis, and stem cell behavior modulation [136].

PET or SPECT imaging of TNC dated back to the 1990s. The primary candidate for PET or SPECT imaging of TNC in cancer is 81C6, a mAb recognizing TNC on gliomas and other tumors [138–141]. In one study, ^{123}I-labeled 81C6 at various doses were used to optimize tumor-to-normal tissue uptake ratio [138]. With the antibody doses ranging from 10 to 100 mg, the distribution of ^{123}I-labeled 81C6 was explored in 16 glioma patients. All tumors were visualized readily by SPECT corresponding to abnormalities from anatomic imaging. Radiation dosimetry calculations found that ~19 Gy of radiation can be delivered to intracranial glioma by injection of 300 mCi of ^{123}I-81C6 with acceptable normal tissue radiation exposure. Combined with possible external beam, ^{123}I-81C6 injection could be useful for radiation therapy of glioma.

Another study was performed to assess the dosimetry of ^{131}I-81C6 in brain tumor patients from direct antibody injections into surgically created resection cavities (SCRCs) [139]. The average retention time of ^{131}I-81C6 in the SCRC was 111 h (65–200 h), with the estimated brain absorbed dose being 6.5 Gy. No neurological toxicity and hematologic toxicity was observed at the maximum tolerated dose. Subsequently, the same research group evaluated dose-response relationships in newly diagnosed brain tumor patients treated with ^{131}I-81C6 into SCRCs accompanied with external-beam radiotherapy and chemotherapy [140]. A preferential distribution of ^{131}I-81C6 through regions of vasogenic edema was observed by MRI/SPECT (Figure 1c). This study confirmed that ^{131}I-81C6 increases the median survival of brain tumor patients. Further clinical studies are warranted to determine the effectiveness of ^{131}I-81C6 in radiation therapy of brain tumors.

Due to the effectiveness of 81C6, human-murine chimeric 81C6 (ch81C6) was further developed and used for the treatment of brain tumor, which was combined with a novel technique named convection-enhanced delivery (CED) [141]. CED can be adopted to transfer agents to the brain parenchyma for the treatment of different brain lesions. The purpose of this study was to determine the efficiency from CED to deliver a larger dose of a radiolabeled mAb compared with a bolus injection. Recurrent glioblastoma multiforme (GBM) patients with positive staining in TNC histological analysis were randomized for an intratumoral injection of ^{123}I-Ch81C6. The results from this study demonstrated that CED did not provide a significant increase in the volume of distribution for the relatively small injected volumes. Due to the high avidity of 81C6 for TNC, Astatine-211 (^{211}At, $t_{1/2}$: 7.2 h) or ^{131}I-labeled 81C6 was successfully adopted for the treatment of primary or metastatic brain tumors (NCT00003461, NCT00002753, and NCT00003478 from clinicaltrials.gov) and the results seemed to be quite promising.

Other TNC-targeting antibodies were also adopted for PET or SPECT imaging of TNC in different cancer models. In one study, a phosphonated acyclic bifunctional chelate was developed and used for the labeling of a mouse mAb (B28-13) for TNC [142]. The labeled antibody maintained the affinity for TNC and possessed high potential for future PET or SPECT imaging and radiotherapy. Another microdosing Phase 0 clinical study was conducted to obtain initial information about pharmacokinetics, biodistribution, and specific tumor targeting of the anti-TNC mini antibody F16SIP (SIP stands for small immunoprotein) [143]. ImmunoPET scans were carried out after injection of ^{124}I-F16SIP into patients with head and neck squamous cell carcinoma. ^{124}I-F16SIP was well tolerated with visible uptake primarily in the liver, spleen, kidneys, and bone marrow which diminished over time. All 4 tumors were visible on 24 h PET images with a good tumor-to-blood ratio of 7.7 ± 1.7 at the time of surgery. Pharmacokinetic analysis revealed good bioavailability of ^{124}I-F16SIP. The results of this study justify further clinical exploration of F16SIP-based therapies, and the effectiveness was confirmed by a recent study using ^{131}I-F16SIP for radioimmunotherapy (RIT) of Hodgkin's lymphoma [144].

Other TNC-targeted molecules such as aptamers were also used for SPECT imaging of TNC [145]. Aptamers are small oligonucleotides screened to bind specifically to a target molecule with high affinity [146]. The aptamer targeting TNC (named TTA1) was prepared and ^{99m}Tc-labeled TTA1 displayed fast blood clearance, rapid tumor penetration, and persistent tumor retention in various solid tumors [145]. As synthetic molecules, aptamers can be readily modified site-specifically. Subsequently, TTA1 was used in another study to generate a multifunctional nanoparticle which can simultaneously detect nucleolin, integrin $\alpha_v\beta_3$ and TNC [147]. Compared with targeting of single receptor, this ^{68}Ga-labeled tri-targeting nanoparticle demonstrated enhanced signal intensity in various cancer types. This nanoparticle could be useful as a broadly applicable probe for the diagnosis of different cancers.

3.7 Eph receptors

Ephrin (Eph) receptors are the largest superfamily of receptor tyrosine kinases [148]. Eph receptor - ephrin signaling is involved in various diseases, particularly in cancer growth and progression [148]. Eph receptors orchestrate a large number of cell-cell interaction events, including but not limited to angiogenesis, tissue development, and neoplastic transformation [149, 150]. Based on the structure features and ephrin binding preferences in human, nine EphA and five EphB subtypes were identified, and they can interact with five type A ephrins and three type B ephrins, respectively [151].

Among all these Eph receptors, the most frequently studied for PET and SPECT imaging include EphA2 [152] and EphB4 [153–156]. EphA2 and EphB4 were reported to be overexpressed in many human tumor tissues such as breast, colon, bladder, prostate, and ovary [148]. Due to their critical functions and widespread expression in these cancer types, Eph receptors-targeted therapies have become a cancer treatment strategy with increasing popularity. Therefore, an efficient imaging modality, such as PET or SPECT, coupled with suitably radiolabeled antibodies or peptides, will provide invaluable insights into the optimization of EphA2- or EphB4-targeted therapies.

To the best of our knowledge, there is only one PET imaging study of EphA2 receptor in the literature [152]. A humanized mAb against EphA2 (named 1C1) was labeled with ^{64}Cu and used for PET imaging in eight tumor models with various EphA2 expression levels. ^{64}Cu-DOTA-1C1 retained superior EphA2 binding affinity/specificity and demonstrated highest uptake in CT-26 tumor with the most abundant expression of EphA2, whereas ^{64}Cu-labeled isotype-matched IgG exhibited background level of tumor uptake (Figure 1d). Excellent linear correlation was corroborated between the tumor uptake from PET imaging and tumor EphA2 expression level measured by Western blotting.

Peptide ligands were the most popular choices for PET or SPECT imaging of EphB4. In 2011, a ^{64}Cu-labeled peptide, TNYLFSPNGPIARAW (TNYL-RAW), which possessed high EphB4 binding affinity, was developed for PET imaging of EphB4 expression in cancer [155]. Strong binding affinity to EphB4 was demonstrated by TNYL-RAW and its derivatives, with a dissociation constant in nM range. Significantly higher uptake of ^{64}Cu-DOTA-TNYL-RAW was showed in PC-3M (EphB4^{+}) and CT-26 (EphB4^{+}) tumors compared with A549 (EphB4^{-}) tumors. Furthermore, blocking experiments by excess amount of TNYL-RAW diminished the uptake of ^{64}Cu-DOTA-TNYL-RAW in both CT-26 and PC-3M tumors, confirming its specificity for EphB4. More recently, dual-labeled TNYL-RAW with both ^{64}Cu and a NIRF dye Cy5.5 was adopted for PET/CT and optical imaging of orthotopic brain tumors in mice [153]. EphB4-specific uptake of the dual-labeled TNYL-RAW peptide was corroborated in both orthotopic U251 (EphB4^{+}) and U87 tumors (EphB4^{-}). Detailed histological examination revealed that the distribution of this peptide was in both tumor blood vessels and tumor cells in U251 tumors, while it only appeared in tumor blood vessels in U87 tumors.

The same peptide sequence was also adopted in the development of a micelle-based nanoplatform for SPECT and NIRF imaging of EphB4 [156]. TNYL-RAW was chemically attached to PEG-coated, core-crosslinked polymeric micelles (CCPM), which were dual-labeled with fluorescent dye Cy7 and ^{111}In. The selectivity of TNYL-RAW-CCPM to EphB4 was confirmed in vitro by cellular assays in PC-3M (EphB4^{+}) and A549 cells (EphB4^{-}). PC-3M tumors were readily detected by both SPECT and NIRF after intravenous administration of ^{111}In-labeled TNYL-RAW-CCPM. In comparison, little signal was observed in A549 tumors injected with the same micelles or in PC-3M tumors injected with ^{111}In-labeled CCPM without TNYL-RAW as the targeting ligand. The EphB4 specificity of ^{111}In-labeled TNYL-RAW-CCPM was further confirmed after co-injection with TNYL-RAW peptide. Histological examination established the correlation between the fluorescence signal and radioactivity from the nanoparticles and the EphB4 expression pattern inside the tissue.

Antibodies for EphB4 can serve as another powerful tool for studying its function in tumor angiogenesis. A series of ^{64}Cu-labeled antibodies was developed and used for PET imaging studies of EphB4 expression in tumors [154]. Anti-EphB4 antibodies (named hAb47 and hAb131) were conjugated with DOTA through lysine (DOTA-Lys-hAb47), cysteine (DOTA-Cys-hAb47), or oligosaccharide (DOTA-Sug-hAb47) on the antibody and DOTA-human IgG (hIgG) without EphB4 binding capacity was used as a control in this study. PET imaging with these probes was conducted in both HT29 and MDA-MB-231 xenografts.

DOTA-Sug-hAb47 demonstrated the highest receptor binding activity in an EphB4 binding assay but ^{64}Cu-DOTA-Sug-hAb47 was trapped in the liver quickly in vivo. Both ^{64}Cu-DOTA-Lys-hAb47 and ^{64}Cu-DOTA-Cys-hAb47 demonstrated prominent tumor accumulation in HT29 xenografts, compared with low tumor accumulation from ^{64}Cu-DOTA-Lys-hIgG. ^{64}Cu-DOTA-Lys-hAb131 was also found to specifically accumulate in the MDA-MB-231 tumor.

Eph receptors and ephrins have been studied extensively to clarify their complex roles in tumor development and progression, nerve injury and tissue regeneration, leading to considerable novel strategies for targeted therapy, with some candidates already in clinical trials [148, 150]. Targeted therapeutics, especially antibodies, ephrin fusion proteins, and small-molecule inhibitors, are being developed to inhibit Eph receptor binding, activation, and relevant signaling. Although Eph receptors are also implicated in a range of neurodegenerative diseases, as well as in inflammatory diseases, strategies for therapeutic targeting in these diseases are only emerging [148]. Imaging of Eph receptors in vivo could therefore be valuable for the sensitive detection of lesions, prognostic evaluation or selection of patients for clinical trials, more accurate treatment monitoring, and mechanism elucidation in a specific treatment.

3.8 c-Met

The proto-oncogene mesenchymal-epithelial transition factor (c-Met) encodes a receptor tyrosine kinase also named hepatocyte growth factor receptor (HGFR), which can originate genetic adjustments resulting in cell growth, cancer invasion and metastasis, and apoptosis protection [157, 158]. It has also been reported that abnormal c-Met expression is more frequently observed in metastases than in primary tumors and is relevant to clinical prognosis [159]. All these findings make c-Met one of the most attractive targets for cancer theranostics.

Developing a radiolabeled tracer to detect c-Met expression would be extremely helpful in the diagnosis and response evaluation of c-Met targeted therapies. DN30 is an antibody that binds to the extracellular portion of c-Met, leading to the retarded growth of tumor xenografts and metastatic spread of cancer cells in mice [160]. With radiolabeled DN30, researchers have demonstrated the potential of using PET imaging for determination of c-Met expression profile in vivo [161]. Tumor targeting with ^{89}Zr-Df-DN30 and ^{124}I-DN30 has been reported in two tumor xenografts: GLT-16 (c-Met^{+}) and FaDu (c-Met^{-}) [161]. Elevated tumor uptake in GLT-16 was confirmed to correlate well with the high expression levels of c-Met in tumors. Interestingly, ^{89}Zr-Df-DN30 showed a significantly higher GLT-16 tumor accumulation in comparison with ^{124}I-labeled counterpart at all time points examined, possibly due to the retention of ^{89}Zr in cells. The successful assessment of in vivo c-Met expression status shown in this study will benefit the selection of the right patient population for DN30-based anti-c-Met therapy, as well as therapeutic response monitoring in future clinical translational research.

In another study, ^{125}I-labeled c-Met-binding peptides (cMBPs) were used for SPECT imaging of c-Met in U87MG (c-Met^{+}) tumor bearing mice. cMBPs were confirmed to possess more effective tumor targeting efficacy for U87MG than other receptor-binding

ligands used in this study. The overall image quality of SPECT/CT was not optimal despite that U87MG tumor xenografts could also be visualized [162]. Following this study, the same group subsequently developed a ^{125}I-labeled cMBP-click-cRGDyk heterodimer to simultaneously target c-Met and integrin $\alpha_v\beta_3$ in vivo [163]. However, cell binding experiments suggested that the cMBP-click-cRGDyk heterodimer maintained only comparable c-Met and integrin $\alpha_v\beta_3$ binding affinities as its corresponding monomer, and no enhanced tumor uptake in vivo was observed [163].

Other antibodies and nanobodies have also been used for targeting c-Met [164–167]. Onartuzumab (~99 kDa, Genentech; under Phase I–III clinical trials) is a humanized monovalent mAb against c-Met with potential anti-neoplastic activity. The antibody possesses nanomolar affinity for c-Met and could prevent the interactions between c-Met and hepatocyte growth factor (HGF, the natural ligand of c-Met), leading to the inhibition of relevant signaling pathways [168].

In a recent study, onartuzumab was radiolabeled with ^{76}Br or ^{89}Zr for PET imaging of tumor c-Met (Figure 1e) [164]. Although in vitro studies showed specific binding for both ^{76}Br-onartuzumab and ^{89}Zr-Df-onartuzumab, in vivo results revealed that ^{89}Zr-Df-onartuzumab was advantageous with significantly higher MKN-45 tumor uptake. The c-Met specificity of ^{89}Zr-Df-onartuzumab was also confirmed by using the U87MG tumor model (low c-Met expression level), where low tumor accumulation was observed. All these indicated that ^{89}Zr-Df-onartuzumab could become an effective immunoPET agent for future patient selection, drug development, treatment monitoring, etc. upon clinical translation. In another study, anti-c-Met nanobodies named 1E2-Alb8 and 6E10-Alb8 were labeled with ^{89}Zr to assess the c-Met expression in vivo [165], and specific tumor uptake of ^{89}Zr-1E2-Alb8 was observed in c-Met positive tumors.

3.9 Extra domain B

Extra domain B (ED-B) is one isoform of fibronectin, and has been known as an important angiogenic marker that is synthesized, secreted, and deposited to the ECM structures from different cell types, including ECs of newly formed blood vessels, myofibroblasts, and, most notably, tumor cells [169, 170]. High levels of ED-B expression have also been detected in both primary tumors and metastatic lesions [171]. In stark contrast, ED-B is almost undetectable in normal tissues, except in tissues undergoing physiological modelling (e.g. endometrium and ovary) or wound healing [172]. All these findings have established ED-B as an attractive target for non-invasive tumor detection and monitoring/predicting the outcome of anti-angiogenic therapies.

Isolated from a phage display library, L19 is a single-chain antibody fragment (scFv) specifically targeting ED-B [173]. Other L19-based immunoconjugates were also constructed, including a dimeric scFv [$(scFv)_2$], a human bivalent SIP (~80 kDa), and a complete human IgG1 [174]. Radioiodines are the most commonly used isotopes to label L19 or its derivatives for ED-B imaging. During the last few years, ^{123}I [171], ^{124}I [175], ^{125}I [174, 176], and ^{131}I [177] labeled L19-SIPs have been reported.

In one of these studies, the suitability of ^{124}I-L19-SIP for detection of early-stage tumor angiogenesis was confirmed, which could be used as a scouting procedure before the adoption of ^{131}I-L19-SIP RIT [175]. Significant uptake of ^{124}I-L19-SIP in tumor was found in the FaDu xenograft and the uptake peaked at 6 h p.i. (Figure 1f). ^{124}I-L19-SIP delineated tumors in a scale of 50 mm^3 and showed no obvious uptake in other organs, paving the way for clinical RIT trials of ^{131}I-L19-SIP [177, 178].

Besides radioiodine-labeled L19, ^{99m}Tc and ^{76}Br are the other isotopes used for generating ED-B targeting tracers [179, 180]. In one study, recombinant and chemically modified derivatives of the scFv L19 were radiolabeled with ^{99m}Tc to form ^{99m}Tc-AP39, ^{99m}Tc-L19-His, and ^{99m}Tc-L19-Hi20 [179]. In comparison with ^{99m}Tc-L19-His and ^{99m}Tc-L19-Hi20, ^{99m}Tc-AP39 showed more prominent and faster tumor uptake, more rapid blood clearance and renal excretion, and higher signal-to-noise ratios in vivo. In another study, fast and specific in vivo targeting of ^{76}Br-L19-SIP was obtained in F9 tumors with slow renal clearance and persistent blood radioactivity [180]. Partial debromination from ^{76}Br-L19-SIP was confirmed in a metabolism study [180]. The specific accumulation of ^{76}Br-L19-SIP in vivo suggests ED-B fibronectin can be an invaluable target for tumor detection by PET.

3.10 VCAM-1

VCAM-1 belongs to the VLA-4 binding immunoglobulin family [181]. It is expressed on activated endothelial or mesothelial cells and plays an important role in the regulation of leukocyte attachment and extravasation during inflammation [182]. The up-regulation of VCAM-1 was observed in different diseases such as severe inflammation [183], atherosclerosis [184], asthma [185], and different types of cancer [186, 187]. Owing to the active participation of VCAM-1 in various diseases, VCAM-1 targeted therapeutic intervention or diagnostic strategies have been extensively investigated.

Tetrameric VCAM-1 targeted peptides were fabricated to monitor the tumor response to platinum-based chemotherapy [188]. This study demonstrated a potential role for VCAM-1 to monitor ovarian cancer peritoneal metastasis and tumor responsiveness to platinum-based chemotherapy. The acquired observations supported the utility of VCAM-1 imaging probes to monitor treatment response in ovarian cancer patients, thus providing the potential to improve patient management. In addition to indicating early metastasis, the ability to detect maximal mesothelial VCAM-1 expression with microscopic tumor burden also has implications for monitoring ovarian cancer patients for recurrence.

3.11 Other vascular targets

PET or SPECT imaging of the above-mentioned major vascular targets can provide invaluable information for diagnosis and treatment monitoring for different types of cancer. Aside from these, several other vascular targets are also important, including the platelet-derived growth factor receptor (PDGFR) [189] and tumor endothelial marker-8 (TEM-8) [190]. However, only a few PET or SPECT imaging studies were carried out for these targets.

The expression levels of PDGFRs correlate with tumor development, invasiveness, and drug resistance, thus posing great influences on clinical prognosis of tumors [189]. Further

knowledge of PDGFR-mediated molecular signaling may provide new insights into the optimization of current cancer therapies and the development of future novel therapeutic regimen. In one study, a fluorinated derivative of PDGFR inhibitor dasatinib (named F-SKI249380) was used for PET imaging to evaluate its delivery and uptake in a high-grade glioma [191]. PDGFR expression level was non-invasively evaluated in vivo using ^{18}F-SKI249380 as well as ^{18}F-SKI249380-containing micellar and liposomal nanoformulations, and apparently higher tumor uptake was observed for the latter. Saturation studies using excess amount of dasatinib resulted in remarkable decrease of tumor uptake, confirming in vivo binding specificity. This ^{18}F-SKI249380-containing micelle may facilitate treatment plans in the future for cancer patients undergoing PDGFR inhibitor therapies.

TEM-8, also named anthrax toxin receptor 1, is a cell surface anthrax toxin receptor [192]. TEM-8 is reported to be selectively over-expressed on both tumor endothelial and cancer cells [190]. Since TEM-8 antagonists and TEM-8-targeted delivery of toxins have been developed as effective anti-cancer strategies, the ability to detect TEM-8 expression fluctuation would be useful for assessing TEM-8-targeted therapies. One example is a 13-meric peptide, KYNDRLPLYISNP (i.e. QQM), identified from the domain IV in protective antigen of anthrax toxin. This QQM peptide was labeled with ^{18}F for PET imaging in both UM-SCC1 (TEM-8^{+}) and MDA-MB-435 (TEM-8^{-}) cancer models [193]. ^{18}F-FP-QQM showed significantly higher accumulation in UM-SCC1 tumors than MDA-MB-435 tumors. This peptide-based tracer is suggested to be a promising lead compound for determination of TEM-8 expression. Further studies to optimize the affinity, specificity and metabolic stability of the tracer are warranted.

4. PET or SPECT imaging of vascular targets in cardiovascular diseases (CVD)

Cardiovascular diseases cause significant morbidity and mortality world-wide. Even though efficient treatments have been developed for specific patient groups, significant amount of cardiovascular diseases are still challenging to treat especially in elderly patients [194]. The maturation of PET or SPECT imaging for different vascular targets will yield new insights into the pathophysiological changes underlying these cardiovascular diseases, which will be discussed below.

4.1 CD105

Recently, radiolabeled TRC105 (i.e. ^{64}Cu-NOTA-TRC105) was used to detect CD105 expression in a murine hindlimb ischemia (HI) model [195, 196], or a rat myocardial infarction (MI) model [197]. It was found that ischemia-induced angiogenesis could be monitored non-invasively with ^{64}Cu-NOTA-TRC105 PET, which showed the highest uptake on day 3 after induction of ischemia (Figure 2a). Blocking studies further confirmed the CD105 specificity of tracer uptake in the ischemic sites [195]. In a subsequent study, we also demonstrated the capability of ^{64}Cu-NOTA-TRC105 in imaging the CD105 expression in a MI model (Figure 2b) [197]. Considering the major challenges in non-invasively assessing ischemia-induced angiogenesis as well as the efficacy of pro-angiogenesis treatment, we believe these two studies will inspire more researchers to use angiogenesis-

targeted agents for identifying the optimal timing of treatment and monitoring the efficacy of therapy in the future.

4.2 Tenascin-C

Due to the vital role of TNC in cardiac and arterial injury, radiolabeled anti-TNC antibodies were chosen for detection of cardiac or arterial diseases such as autoimmune myocarditis [198], MI [199], or cardiac repair after acute MI [200]. Due to the invasiveness and inferior sensitivity of biopsy test in myocarditis diagnosis, a new diagnostic technique was developed in 2002 for the early detection of myocarditis using TNC as a molecular marker [198]. In this study, ^{111}In-labeled anti-TNC mAb Fab fragment was injected into a rat model of experimental autoimmune myocarditis (EAM), monitored by SPECT for its in vivo biodistribution. Rapid blood clearance was observed and the elevated uptake of ^{111}In anti-TNC Fab was clearly demonstrated at locations which did not have significant uptake of ^{99m}Tc-methoxyisobutyl isonitrile (MIBI, a commonly used tracer for myocardial perfusion imaging [201]) (Figure 2c).

Enhanced TNC expression was also observed during the cardiac recovery after MI, which prompted another research group to develop a radiolabeled scFv against TNC for in vivo imaging of MI [199]. The scFv for TNC (named 4F10) was expressed in E. coli and had nM binding affinity. Site-specific ^{111}In labeling was achieved via introduction of a chelating group onto a cysteine residue. After administering of ^{111}In-4F10 into a rat model of acute MI, significantly radioactivity accumulation was observed at the infarcted myocardium than the non-infarcted. Following similar strategy, cardiac repair evaluation was carried out at the early stage of left ventricular remodeling using an ^{111}In-anti-TNC-Fab, generated from a mAb for TNC [200]. Autoradiography and dual-isotope SPECT were performed with both ^{111}In-anti-TNC-Fab and ^{99m}Tc-MIBI. SPECT imaging confirmed that the regional myocardial uptake of ^{111}In-anti-TNC-Fab was complementary to the perfusion pattern from MIBI. The results indicated that localization of the infarcted region can be detected by ^{111}In-anti-TNC-Fab, suggesting its potential use for cardiac repair detection.

Targeting/imaging of TNC in different diseases offers two major advantages: 1) TNC is found to express primarily in damaged tissues, vascular diseases, and a majority of malignant solid tumors [202], which may lead to high specificity for disease detection; 2) it can provide insight on not only injury but also repair of the diseases [199].

4.3 P-selectin

Selectins are a protein family composed of Ca^{2+}-dependent carbohydrate binding proteins which are critical for leukocyte recruitment in the inflammatory process [203]. Blocking of selectins is therefore considered a promising approach to treat acute or chronic inflammatory diseases. Depending on the site of expression, they can be classified into E-selectin (activated endothelium), P-selectin (platelets and ECs), and L-selectin (lymphocytes) [204].

P-selectin has been well characterized and demonstrated as a potential target for thrombus diagnosis and therapy [205, 206]. P-selectin is usually involved in inflammatory disorders (e.g. acute lung injury, psoriasis, and rheumatoid arthritis) but it also participates in hemostasis and metastasis of tumor cells [207]. Furthermore, high expression level of P-

selectin is relevant to the pathological transformation of arterial thrombus and EC activation after a transient ischemia, making it an attractive target in various cardiovascular diseases. Recently, much effort has been devoted to the development of imaging agents that target P-selectin [206, 208, 209].

In one study, the light chain (LC) of SZ-51 (a mouse mAb against human P-selectin [210]) was expressed in *P. pastoris* [206]. SZ-LC was shown to bind activated platelet specifically. Using ^{99m}Tc-MAG3-SZ-LC, the fresh thrombus induced in dog was clearly visualized via SPECT (Figure 2d), indicating that radiolabeled SZ-LC could become a promising new tracer for specific imaging of thrombus [206]. The difference of *in vitro* and *in vivo* binding affinity between intact SZ-51 antibody and SZ-LC, however, were not provided in the report. Accurate diagnosis of acute pulmonary injury remains a major challenge, which could not be achieved without significant improvement in imaging techniques or the development of appropriate imaging agents. Besides imaging thrombus in vivo, in another study, ^{99m}Tc-SZ-51-(Fab′)$_2$ was generated for the detection of pulmonary embolism by SPECT [209].

^{99m}Tc-labeled fucoidan (a polysaccharidic ligand of P-selectin with nM affinity and very low non-specific binding [211]) was developed for the detection of P-selectin expression in two clinically relevant experimental models (i.e. platelet rich arterial thrombi and myocardial ischemia-reperfusion), both of which are associated with over-expression of P-selectin [208]. It was found that ^{99m}Tc-fucoidan SPECT was able to detect the platelet-rich arterial thrombi, vegetations of endocarditis, and mural aneurysmal thrombus [208].

A recent study also showed that P-selectin from human atherosclerotic plaques [212] could regulate the recruitment of monocytes and lymphocytes [213], making radiolabeled anti-P-selectin antibody an attractive option for sensitive detection of atherosclerotic plaques. By using a commercially available anti-mouse P-selectin mAb, i.e. RB40.34, early detection of atherosclerotic plaques by PET/CT was achieved [214]. Selective and prominent uptake of ^{64}Cu-DOTA-RB40.34 in the aortic root from Ldlr−/− mice (fed with a high cholesterol diet for induction of atherosclerotic plaque) was observed and confirmed with ex vivo biodistribution studies. Meanwhile, significantly lower level of the probe was detected in the control group. Oil red O staining and ex vivo autoradiography of aortas were also performed to further confirm the probe accumulation in atherosclerotic plaques.

4.4 VCAM-1

Besides targeting VCAM-1 in different cancer models, another important function of VCAM-1 targeted imaging is the detection of cardiovascular diseases, especially atherosclerosis. PET/CT was used to image VCAM-1 in atherosclerosis with a peptidic tracer called ^{18}F-4V [215]. This technique can detect VCAM-1 expression in murine aortas, considerably smaller than epicardial human coronary arteries. Targeting of VCAM-1 was also demonstrated to be useful for imaging of other cardiovascular diseases. For example, a nanobody (the smallest possible [10–15 kDa] functional immunoglobulin-like antigen-binding fragment [216] derived from unique heavy-chain-only antibodies) for VCAM-1 named cAbVCAM1-5 was generated and evaluated for preclinical imaging of atherosclerotic plaques [217]. The heat resistance of developed nanobodies facilitated

its ^{99m}Tc-labeling and resulted in high radiochemical yield and purity. In ApoE$^{-/-}$ atherosclerotic mice, VCAM-1-positive lesions were readily identified by SPECT/CT using ^{99m}Tc-cAbVCAM1-5, which provided the foundation for future clinical translation.

Peptidic VCAM-1 ligands were also developed for detection of VCAM-1 expression in atherosclerosis. For example, VCAM-1 ligands called B2702-p and B2702-rp were radiolabeled with ^{123}I or ^{99m}Tc to detect atherosclerotic plaques in a rabbit model of atherosclerosis [218]. B2702-p and B2702-rp derive from the linear sequences of a major histocompatibility complex I (MHC-I) molecule with profound immunomodulatory effects. The inhibition of leucocyte recruitment by B2702-rp was confirmed by direct interaction with VCAM-1. The derivatives of B2702-p with optimized target-to-background ratio were subsequently developed, generating improved SPECT image quality in atherosclerotic lesions [219].

5. PET or SPECT imaging of vascular targets in inflammation

Imaging of inflammation has been quite challenging in the past. Despite the fact that FDG is well known to be taken up in inflammation, more agents are needed due to its low specificity for inflammation detection [220], and till date the quest to find optimal imaging agents is still ongoing [221]. PET or SPECT imaging of various vascular targets that are involved in inflammation can pave the way to this ultimate goal. Even though ^{18}F-FDG, the most widely-used PET tracer in clinic, is well-known to accumulate in inflammatory tissue, the uptake is generally not inflammation specific, thus the development of tracers with improved specificity is of importance.

5.1 E-selectin

E-selectin (also known as endothelial-leukocyte adhesion molecule -1 [ELAM-1]) is implicated in the pathogenesis of RA, and its expression level is increased in the inflamed synovial endothelium [222]. Radiolabeled mAb for E-selectin (e.g. 1.2B6) and its Fab fragment have been developed and used for PET or SPECT imaging of RA in pigs or human patients [223–225].

With the aim to determine whether the SPECT/CT could be used to detect E-selectin expression, ^{111}In-DTPA-1.2B6 was used for imaging of human synovial tissue transplants into immune system compromised mice [226]. Representative SPECT/CT fused images showed significantly higher uptake of ^{111}In-DTPA-1.2B6 in the transplants in comparison with the control antibody at 24 h p.i. (Figure 3a). However, several limitations still exist in regards to the model used, which deserves further improvement in the future. First, the synovium was not imaged in the real joint surrounding. Second, the expression level of inflammatory molecules could be significantly different between fresh and transplanted synovium.

E/P-selectin has a well-documented role in regulating inflammation reactions as well as in many other diseases such as cardiovascular diseases and cancer. Different strategies were used to regulate E/P-selectin-mediated functions via blocking the interaction with their ligands, inhibiting the synthesis of its ligands, and preventing the formation of selectin

carbohydrate binding determinants [203] for controlling cell adhesion in inflammation and metastasis. New ligands for E/P-selectin have been developed recently [203, 204], which could be used for future targeted imaging and therapy of different diseases. PET or SPECT imaging could be used to confirm their specificity and optimize their targeting efficacy before further clinical studies.

5.2 Vascular adhesion protein-1

Vascular adhesion protein-1(VAP-1) is a glycoprotein from ECs and it participates in inflammatory reaction via rapid translocation from the intracellular storage granules to the EC surface [227]. It contributes to the extravasation cascade and controls trafficking of different immune cells to locations of inflammation. VAP-1 has a dual function as an adhesin and an amine oxidase [227], which establishes its distinct role from other conventional adhesion molecules. By catalysis of oxidative deamination of primary amines, generation of highly potent inflammatory mediators (e.g. hydrogen peroxide, aldehyde, and ammonium) [228], and interaction with other adhesion molecules (e.g. E/P-selectin, ICAM-1 and VCAM-1) [229], VAP-1 participates in the development of various diseases and is usually up-regulated on the vasculature [230, 231]. All these features supported VAP-1 as a highly promising target molecule to study angiogenic/inflammatory processes in vivo by PET or SPECT.

^{68}Ga-labeled VAP-1 targeting peptide (^{68}Ga-DOTA-VAP-P1) could provide sensitive detection of early inflammatory responses and infection-related processes [232]. In a pilot study, PET imaging was carried out in Sprague-Dawley rats with Staphylococcus aureus induced tibial osteomyelitis or healing cortical bone defects (as a control model of inflammatory responses within a healing process) using ^{68}Ga-DOTA-VAP-P1 as the tracer (Figure 3b) [233]. Significant uptake of ^{68}Ga-DOTA-VAP-P1 in both the osteomyelitic bones and the healing bone defects was shown during early stage after surgery (0 – 36 h), whereas only the osteomyelitic tibias could be delineated afterwards. The osteomyelitic and control animals showed a significant difference at 7 days after surgery. This study validated the capability of ^{68}Ga-DOTA-VAP-P1 for accurate demonstration of the inflammation phase and bacterial infection progress. In this context, ^{68}Ga-DOTA-VAP-P1 was later adopted in healthy rats and rats with bone inflammation for detection of inflammation induced by Staphylococcus aureus infection [233]. With rapid clearance from blood, ^{68}Ga-DOTA-VAP-P1 demonstrated modest target-to-background ratio when compared with those from the control peptide and ^{68}Ga-DOTA-VAP-P1 plus competitors. The utilization of ^{68}Ga-DOTA-VAP-P1 is an important initial step for future development of VAP-1-specific imaging agents.

After the confirmation of its specificity to VAP-1 in vivo, ^{68}Ga-DOTA-VAP-P1 was evaluated in another study for comparison with ^{18}F-FDG (Figure 3c) [234]. Rats with both subcutaneous pancreatic cancer xenografts and acute sterile inflammation were used in this study. ^{68}Ga-DOTA-VAP-P1 demonstrated superior delineation of inflammation over ^{18}F-FDG, with no interfering tumor uptake like ^{18}F-FDG. Immunohistochemistry confirmed increased VAP-1 expression at the inflammatory site with undetectable level in the tumor. It was concluded that ^{68}Ga-DOTA-VAP-P1 was able to visualize inflammation specifically.

Chemical modification of VAP-P1 was subsequently investigated to generate more advantageous imaging agents. To prolong the metabolic half-life of ^{68}Ga-DOTA-VAP-P1, a new analog of ^{68}Ga-DOTA-VAP-P1 was developed with the inclusion of a PEG spacer (i.e. ^{68}Ga-DOTA-VAP-PEG-P1) for in vivo imaging of inflammation [235]. Visualization of inflammation was performed in a rat model with both ^{68}Ga-DOTA-VAP-P1 and ^{68}Ga-DOTA-VAP-PEG-P1. In vivo stability of the two peptides was analyzed by radio-HPLC. Slower renal excretion but similar liver uptake was identified for ^{68}Ga-DOTA-VAP-PEG-P1 compared with ^{68}Ga-DOTA-VAP-P1. Higher target-to-background ratios were achieved from the prolonged metabolic half-life of peptide via PEG spacer, leading to improved imaging quality of inflammation.

Besides VAP-P1, other new ligands for VAP-1 with optimized characteristics were also actively pursued. A cyclic 17-mer peptide from phage display selection was conjugated with DOTA via PEG linker and labeled with ^{68}Ga (called ^{68}Ga-DOTA-VAP-PEG-P2) [236]. ^{68}Ga-DOTA-VAP-PEG-P2 could be cleared rapidly from blood and with an excretion from urine in rats. The enhanced stability of ^{68}Ga-DOTA-VAP-PEG-P2 when compared with ^{68}Ga-DOTA-VAP-P1 warranted its further investigations in vivo. In addition, another candidate named Siglec-9 was also developed by the same group via phage display [237]. The binding between Siglec-9 and VAP-1 was confirmed and the enzymatic groove of VAP-1 was identified to be the interaction site. Specific detection of VAP-1 at sites of inflammation and cancer was achieved by ^{68}Ga-labeled Siglec-9.

Antibody for VAP-1 was another indispensable tool for PET or SPECT imaging of VAP-1. BTT-1023 is an anti-VAP-1 mAb for the treatment of inflammatory diseases. In a recent study, radioiodinated BTT-1023 was adopted for inflammation imaging in a rabbit model of arthritis [238]. Pharmacokinetics of ^{124}I-BTT-1023 was elucidated by PET/CT up to 72 h after injection. Rabbits with chemically induced synovitis were imaged with ^{123}I-BTT-1023 SPECT/CT [238]. Radioiodinated BTT-1023 cleared rapidly from blood circulation and distributed to liver and thyroid. Importantly, ^{123}I-BTT-1023 can delineate the inflamed joint in the rabbit which confirmed its capacity to detect mild inflammation in vivo. Clinical ^{124}I-BTT-1023 PET studies may be justified with proper design of injection dose.

Generally speaking, VAP-1 targeted agents could be valuable not only for the diagnosis and treatment planning for patients with inflammatory conditions, such as RA, but also for the drug discovery processes. In addition to therapy monitoring and stratification of patients for specific anti-inflammatory treatment, imaging of VAP-1 could also be a scientific tool for in vivo investigation of leukocyte trafficking in inflammatory sites.

5.3 VCAM-1

The primary application of VCAM-1 targeted imaging is the detection of inflammation. A ^{123}I-labeled anti-VCAM-1 antibody was used to evaluate its usefulness in the assessment of colitis [239], which demonstrated the usefulness of SPECT imaging to evaluate the inflammatory activity in an experimental model of colitis in the rat. Inflamed colon could be identified on scintigraphy of colitic rats, whereas there was no significant tracer activity in control animals. The important role of VCAM-1 in the progression of inflammatory vascular lesions and its easy access render this molecule an attractive imaging target. In

inflammation, imaging of VCAM-1 presents high specificity for the diagnosis since significant endothelial expression of VCAM-1 is generally restricted to inflamed tissues [240]. Therefore, imaging of VCAM-1 can offer tremendous advantages over the gold standard for SPECT imaging of inflammation, ^{99m}Tc-HMPAO-labeled leukocyte scintigraphy [239]. In cardiovascular diseases, its early induction, selective expression, and easy accessibility from the blood pool strongly suggested that VCAM-1 is an attractive imaging biomarker [241].

6. Conclusion and future perspectives

Different imaging techniques have been applied for collecting structural, functional and molecular information inside tissue vasculature from pathological angiogenesis, many of which have served as indispensable tools in anti-angiogenic drug evaluation. Due to the high sensitivity and high tissue penetration capacity, PET or SPECT will probably provide the highest clinical relevance in this aspect for widespread use in future clinical scenarios [17, 39, 49]. Moreover, the toxicity concerns of PET or SPECT tracers are alleviated when compared to CT, MRI or ultrasound imaging agents since much lower amount are needed for PET or SPECT imaging, despite the radioactivity exposure to the patients. Early detection of disease, patient stratification, and therapeutic outcome monitoring compose the core value of molecular imaging in patient management. These PET or SPECT tracers have the potential to select patients who can benefit from a specific anti-angiogenic treatment (e.g. for cancer treatment) or pro-angiogenic treatment (e.g. for a cardiovascular disease treatment) and be used to track therapeutic responses from these angiogenesis-targeted drugs.

Many factors need to be considered when choosing the optimal vascular targets for in vivo imaging. The complex and dynamic network between different angiogenic factors dominates the sprout of new vessels [13, 29], which usually means that level changes of one specific factor should be readily compensated by others in the normal situation. The “normal” angiogenesis differs from pathological angiogenesis in the tightly regulated balance between these angiogenesis-relevant molecules, whereas such balance is lost in the latter. The considerable heterogeneity of vascular targets, which can vary at different stages of disease, provided researchers the opportunities to find the right target(s) for therapeutic/diagnostic purposes. For example, high levels of VEGFRs can be found on the ECs of vessels which provide the nutrient supply to solid tumors [19]. Although the expression profile of VEGF/VEGFR at a given time point can be determined by histological examination, PET or SPECT imaging could non-invasively acquire more accurate dynamic information of heterogeneous pattern of the targets for longitudinal measurements..

A large number of vascular targets have been identified in different diseases. Despite the fact that no disease is originated from one factor, it is also true that certain factor may be dominant for a specific disease in an individual patient. The vascular targets listed in this review (Table 1) have different applicability in different diseases. The abundant expression of VEGFR, integrins or CD105 on activated ECs makes them attractive targets for detection of both cancer and cardiovascular diseases [21, 52, 92]. The universal expression of MMPs in different diseases (cancer, inflammation, cardiovascular diseases) enables it to serve as a

versatile target for therapeutic intervention. However, the comparatively low affinity and high non-specific tissue uptake of MMPIs in vivo undermined their pertinence in PET or SPECT imaging [134]. Despite the early discovery of TNC [202], Eph receptors [148], c-Met [242], and ED-B [243] in cancer biology, PET or SPECT imaging of these targets is still in its infancy. Although different clinical trials focused on these targets have already been initiated, further optimization of existing ligands or development of new ligands will still be needed. For imaging of inflammatory diseases, the targeting agents for E/P-selectins [204, 207], VAP-1 [230] and VCAM-1 [183] are the mainstay. In addition, there are many other attractive targets which need further attention and future investigation. For example, despite their critical roles in angiogenesis, no PET or SPECT imaging of Tie receptors has been reported to date [33].

A diverse array of imaging agents have been developed for aforementioned vascular targets including antibody/antibody fragments, peptides, small-molecule inhibitors, aptamers, nanomaterials, etc. Future studies need to be carried out to carefully explore the pharmacokinetics, toxicity, and certain other properties (e.g. immune response) of these imaging agents, which can help identify the optimal tracers for clinical translation. Another potentially beneficial strategy is the generation of bispecific or multispecific imaging agents, which can bind to two or multiple targets at the same time to enhance the detection specificity.

Despite the general assumption that imaging results correlate with the target expression level in vivo, this conclusion has not been extensively validated. In most studies, PET or SPECT imaging in two tumor models, one positive control and one negative, was carried out. Quantitative correlation between the in vivo target expression level and the non-invasive imaging data is rare [152], but such validation is especially critical for therapeutic response monitoring, as it is the pre-requirement for the researchers/clinicians adopting the imaging techniques to monitor the target expression level in each individual patient over time. Lack of accurate quantification is one of the major reasons that very few PET or SPECT tracers perform well in the clinical setting.

One disadvantage of PET or SPECT is the inherently low spatial resolution. Hybrid systems, like PET/CT, SPECT/CT, PET/MRI, and SPECT/MRI can provide partial solutions for this issue and play a leading role in future angiogenesis imaging. These hybrid imaging systems will potentially smooth translational research from experimental animal studies into clinical investigation and practice. High sensitivity of PET or SPECT can be co-registered with high resolution CT/MRI to accurately identify and quantify radiotracer uptake. Another limitation for future application of nuclear imaging is the radiation exposure. In a study comparing the risks of cumulative cancer incidence from digital mammography and PET (or SPECT), the numbers from PET (e.g. 370 MBq of ^{18}F-FDG) or SPECT (e.g. 925 MBq of ^{99m}Tc labeled sestamibi) are 15–30 times higher [244]. Careful optimization of in vivo pharmacokinetics of the tracers and introduction of more desirable radioisotopes are still essential for minimizing the radiation exposure. In addition, development of PET or SPECT tracers with relatively long decay half-lives (e.g. a few days) may be more financially suitable for future clinical use. A longer half-life can facilitate the transportation of radiotracers between

different laboratories and clinics, obviating the necessity of an on-site cyclotron in every imaging center.

To further improve imaging of angiogenesis, it is essential to both identify new vascular targets/specific ligands and optimize existing reagents. Further understanding of angiogenic cascades will add bricks to new target identification. Optimization of currently available imaging probes can also be carried out using different strategies. First, oligomerization of the targeting ligand (small-molecule inhibitors, peptides, or small-size proteins) can improve the receptor binding and target retention benefiting from polyvalency effect. Second, site-specific labeling of the targeting ligands will be more advantageous than random modifications on lysine residues to maintain the binding affinity and functional activity. Third, choosing of an appropriate linker between the ligand and the radiolabel can sometimes improve the pharmacokinetics. Strategies like PEGylation, glycosylation, and different other linkers have been confirmed to improve the imaging quality [245]. Last, new strategies should be required to improve the labeling yield (especially for ^{18}F-based imaging agents).

The chemical modification of these PET or SPECT reagents will significantly affect their tissue distribution. At the same time, the chemical component of PET or SPECT tracers is also crucial for their bioavailability in vivo. Depending on the category of the tracer, they can have different tissue penetration, diffusive character, plasma protein binding capacity, cell internalization, and capability to penetrate the blood brain barrier (BBB). For small-molecule TKIs, despite their high affinities for the receptors, they tend to display high protein binding due to their hydrophobicity. Peptide- or small protein- based PET or SPECT tracers can have fast tissue penetration (particularly in a cancerous tissue) and prompt cellular internalization upon the binding of their receptors, but their active interaction with plasma enzymes renders their low stability in vivo. Antibodies are comparatively stable in vivo and they usually possess a long circulation half-life, which can result in high accumulation in disease region if sufficient time is given. However, the larger molecular size renders them difficult to pass through BBB except in certain scenarios with compromised BBB. Nanomaterials-based PET or SPECT tracers can combine the advantages of different ligands but their interaction with mononuclear phagocyte system (result in high liver/spleen accumulation) will raise toxicological concerns. To improve the bioavailability of these tracers, collaborative efforts are needed, which rely on biologists to identify and validate new targets, chemists/engineers to synthesize and characterize the ligands with suitable applicability in different diseases.

Different labeling strategies were also adopted for the production of angiogenic markers-targeted PET or SPECT imaging agents with improved affinity or specificity to their targets. Since significant amount of imaging agents introduced in this review article involved the use of radiometals, various new chelating compounds have been developed for stabilization of radiometals on the imaging agent. Compared with commonly used chelating compounds such as DOTA or NOTA, ligands like NODAGA [246] or CB-TE1A1P [86] can benefit from a decreased tracer uptake in normal tissues. At the same time, site-specific radiolabeling [61] can minimize the bioactivity loss of imaging agents. An ideal radiolabeling scheme is to create a fast, location-selective introduction of radioisotope into

the target molecule with a high yield and under mild conditions. Following those rules, different “click chemistry” strategies using cycloaddition reactions can be useful tools for radiolabeling, especially for reactions participated by ^{18}F [247].

Most of the molecular imaging probes suffer from the slow clinical translation from bench to bedside. Multiple factors in tracer development, e.g. the investigational new drug (IND)-directed toxicology, significantly slow down the translational process. The high specificity (targeting efficiency) required for PET or SPECT tracers not only leads to higher costs of development but also limits their target population, which is a risk factor for the investors. However, the situation has been improved by wider availability of scanners, easier access to small animal studies, and the option of exploratory IND mechanism from the FDA to enable faster first-in-human studies. PET or SPECT imaging can serve as a bridge between preclinical and clinical research to screen higher target specificity and improved pharmacodynamics. It is expected that imaging of angiogenesis with PET or SPECT tracers will be routinely applicable in future clinical practice.

In summary, PET and SPECT imaging can provide molecularly targeted approaches for the early assessment of biological events that precede the physiological or anatomical signature of a disease. These imaging techniques offer unique opportunities for evaluation of pathogenesis, progression, and therapeutic intervention. The continuing development of more sensitive and specific PET and SPECT tracers will confirm the delivery of therapeutic (anti-)angiogenic agents and directly monitor progression of angiogenesis within targeted tissues, providing novel methods for optimizing therapeutic interventions in patients suffering from various forms of disease.

Acknowledgments

The authors are grateful for financial support from the University of Wisconsin - Madison, the National Institutes of Health (NIBIB/NCI 1R01CA169365 and P30CA014520), the Department of Defense (W81XWH-11-1-0644), and the American Cancer Society (125246-RSG-13-099-01-CCE).

References

1. Griffioen AW, Molema G. Angiogenesis: potentials for pharmacologic intervention in the treatment of cancer, cardiovascular diseases, and chronic inflammation. Pharmacol Rev. 2000; 52:237–268. [PubMed: 10835101]
2. Goel S, Duda DG, Xu L, Munn LL, Boucher Y, Fukumura D, Jain RK. Normalization of the vasculature for treatment of cancer and other diseases. Physiol Rev. 2011; 91:1071–1121. [PubMed: 21742796]
3. Pepper MS. Role of the matrix metalloproteinase and plasminogen activator-plasmin systems in angiogenesis. Arterioscler Thromb Vasc Biol. 2001; 21:1104–1117. [PubMed: 11451738]
4. Siefert SA, Sarkar R. Matrix metalloproteinases in vascular physiology and disease. Vascular. 2012; 20:210–216. [PubMed: 22896663]
5. Mitsos S, Katsanos K, Koletsis E, Kagadis GC, Anastasiou N, Diamantopoulos A, Karnabatidis D, Dougenis D. Therapeutic angiogenesis for myocardial ischemia revisited: basic biological concepts and focus on latest clinical trials. Angiogenesis. 2012; 15:1–22. [PubMed: 22120824]
6. Annex BH. Therapeutic angiogenesis for critical limb ischaemia. Nat Rev Cardiol. 2013; 10:387–396. [PubMed: 23670612]
7. Bergers G, Benjamin LE. Tumorigenesis and the angiogenic switch. Nat Rev Cancer. 2003; 3:401–410. [PubMed: 12778130]

8. Sluimer JC, Daemen MJ. Novel concepts in atherogenesis: angiogenesis and hypoxia in atherosclerosis. J Pathol. 2009; 218:7–29. [PubMed: 19309025]
9. Szekanecz Z, Besenyei T, Szentpetery A, Koch AE. Angiogenesis and vasculogenesis in rheumatoid arthritis. Curr Opin Rheumatol. 2010; 22:299–306. [PubMed: 20305562]
10. Costa PZ, Soares R. Neovascularization in diabetes and its complications. Unraveling the angiogenic paradox. Life Sci. 2013; 92:1037–1045. [PubMed: 23603139]
11. Vijaynagar B, Bown MJ, Sayers RD, Choke E. Potential role for anti-angiogenic therapy in abdominal aortic aneurysms. Eur J Clin Invest. 2013; 43:758–765. [PubMed: 23672465]
12. Rabquer BJ, Koch AE. Angiogenesis and vasculopathy in systemic sclerosis: evolving concepts. Curr Rheumatol Rep. 2012; 14:56–63. [PubMed: 22083296]
13. Noonan DM, De Lerma Barbaro A, Vannini N, Mortara L, Albini A. Inflammation, inflammatory cells and angiogenesis: decisions and indecisions. Cancer Metastasis Rev. 2008; 27:31–40. [PubMed: 18087678]
14. Kim YW, West XZ, Byzova TV. Inflammation and oxidative stress in angiogenesis and vascular disease. J Mol Med (Berl). 2013; 91:323–328. [PubMed: 23430240]
15. Kundu JK, Surh YJ. Emerging avenues linking inflammation and cancer. Free Radic Biol Med. 2012; 52:2013–2037. [PubMed: 22391222]
16. Costa C, Incio J, Soares R. Angiogenesis and chronic inflammation: cause or consequence? Angiogenesis. 2007; 10:149–166. [PubMed: 17457680]
17. Stacy MR, Maxfield MW, Sinusas AJ. Targeted molecular imaging of angiogenesis in PET and SPECT: a review. Yale J Biol Med. 2012; 85:75–86. [PubMed: 22461745]
18. Ferrara N. Vascular endothelial growth factor: basic science and clinical progress. Endocr Rev. 2004; 25:581–611. [PubMed: 15294883]
19. Olsson AK, Dimberg A, Kreuger J, Claesson-Welsh L. VEGF receptor signalling - in control of vascular function. Nat Rev Mol Cell Biol. 2006; 7:359–371. [PubMed: 16633338]
20. Fagiani E, Christofori G. Angiopoietins in angiogenesis. Cancer Lett. 2013; 328:18–26. [PubMed: 22922303]
21. Barczyk M, Carracedo S, Gullberg D. Integrins. Cell Tissue Res. 2010; 339:269–280. [PubMed: 19693543]
22. Harshman LC, Choueiri TK. Targeting the hepatocyte growth factor/c-Met signaling pathway in renal cell carcinoma. Cancer J. 2013; 19:316–323. [PubMed: 23867513]
23. Heldin CH. Targeting the PDGF signaling pathway in tumor treatment. Cell Commun Signal. 2013; 11:97. [PubMed: 24359404]
24. Welti J, Loges S, Dimmeler S, Carmeliet P. Recent molecular discoveries in angiogenesis and antiangiogenic therapies in cancer. J Clin Invest. 2013; 123:3190–3200. [PubMed: 23908119]
25. Ribatti D, Ranieri G, Basile A, Azzariti A, Paradiso A, Vacca A. Tumor endothelial markers as a target in cancer. Expert Opin Ther Targets. 2012; 16:1215–1225. [PubMed: 22978444]
26. Wang Z, Yan X. CD146, a multi-functional molecule beyond adhesion. Cancer Lett. 2013; 330:150–162. [PubMed: 23266426]
27. Principe DR, Doll JA, Bauer J, Jung B, Munshi HG, Bartholin L, Pasche B, Lee C, Grippo PJ. TGF-beta: duality of function between tumor prevention and carcinogenesis. J Natl Cancer Inst. 2014; 106:djt369. [PubMed: 24511106]
28. Folkman J. Angiogenesis: an organizing principle for drug discovery? Nat Rev Drug Discov. 2007; 6:273–286. [PubMed: 17396134]
29. Potente M, Gerhardt H, Carmeliet P. Basic and therapeutic aspects of angiogenesis. Cell. 2011; 146:873–887. [PubMed: 21925313]
30. Bonauer A, Boon RA, Dimmeler S. Vascular microRNAs. Curr Drug Targets. 2010; 11:943–949. [PubMed: 20415654]
31. Crawford Y, Ferrara N. VEGF inhibition: insights from preclinical and clinical studies. Cell Tissue Res. 2009; 335:261–269. [PubMed: 18766380]
32. Crawford Y, Ferrara N. Tumor and stromal pathways mediating refractoriness/resistance to anti-angiogenic therapies. Trends Pharmacol Sci. 2009; 30:624–630. [PubMed: 19836845]

33. Eroglu Z, Stein CA, Pal SK. Targeting angiopoietin-2 signaling in cancer therapy. Expert Opin Investig Drugs. 2013; 22:813–825.
34. Jeltsch M, Leppanen VM, Saharinen P, Alitalo K. Receptor tyrosine kinase-mediated angiogenesis. Cold Spring Harb Perspect Biol. 2013; 5
35. Scaringi C, Minniti G, Caporello P, Enrici RM. Integrin inhibitor cilengitide for the treatment of glioblastoma: a brief overview of current clinical results. Anticancer Res. 2012; 32:4213–4223. [PubMed: 23060541]
36. Ebos JM, Kerbel RS. Antiangiogenic therapy: impact on invasion, disease progression, and metastasis. Nat Rev Clin Oncol. 2011; 8:210–221. [PubMed: 21364524]
37. Mankoff DA. A definition of molecular imaging. J Nucl Med. 2007; 48:18N, 21N.
38. James ML, Gambhir SS. A molecular imaging primer: modalities, imaging agents, and applications. Physiol Rev. 2012; 92:897–965. [PubMed: 22535898]
39. Cai W, Chen X. Multimodality molecular imaging of tumor angiogenesis. J Nucl Med. 2008; 49(Suppl 2):113S–128S. [PubMed: 18523069]
40. Zhu L, Niu G, Fang X, Chen X. Preclinical molecular imaging of tumor angiogenesis. Q J Nucl Med Mol Imaging. 2010; 54:291–308. [PubMed: 20639815]
41. Haubner R, Beer AJ, Wang H, Chen X. Positron emission tomography tracers for imaging angiogenesis. Eur J Nucl Med Mol Imaging. 2010; 37(Suppl 1):S86–103. [PubMed: 20559632]
42. Stacy MR, Zhou W, Sinusas AJ. Radiotracer imaging of peripheral vascular disease. J Nucl Med. 2013; 54:2104–2110. [PubMed: 24101686]
43. Orbay H, Hong H, Zhang Y, Cai W. PET/SPECT imaging of hindlimb ischemia: focusing on angiogenesis and blood flow. Angiogenesis. 2013; 16:279–287. [PubMed: 23117521]
44. Peremans K, Cornelissen B, Van Den Bossche B, Audenaert K, Van de Wiele C. A review of small animal imaging planar and pinhole spect Gamma camera imaging. Vet Radiol Ultrasound. 2005; 46:162–170. [PubMed: 15869162]
45. Berman DS, Kiat H, Van Train K, Friedman JD, Wang FP, Germano G. Dual-isotope myocardial perfusion SPECT with rest thallium-201 and stress Tc-99m sestamibi. Cardiol Clin. 1994; 12:261–270. [PubMed: 8033176]
46. Phelps ME, Hoffman EJ, Mullani NA, Ter-Pogossian MM. Application of annihilation coincidence detection to transaxial reconstruction tomography. J Nucl Med. 1975; 16:210–224. [PubMed: 1113170]
47. Price EW, Orvig C. Matching chelators to radiometals for radiopharmaceuticals. Chem Soc Rev. 2014; 43:260–290. [PubMed: 24173525]
48. Siegel R, Ma J, Zou Z, Jemal A. Cancer statistics, 2014. CA Cancer J Clin. 2014; 64:9–29. [PubMed: 24399786]
49. Dijkgraaf I, Boerman OC. Molecular imaging of angiogenesis with SPECT. Eur J Nucl Med Mol Imaging. 2010; 37(Suppl 1):S104–113. [PubMed: 20617435]
50. Ferrara N. VEGF and the quest for tumour angiogenesis factors. Nat Rev Cancer. 2002; 2:795–803. [PubMed: 12360282]
51. Hicklin DJ, Ellis LM. Role of the vascular endothelial growth factor pathway in tumor growth and angiogenesis. J Clin Oncol. 2005; 23:1011–1027. [PubMed: 15585754]
52. Cai W, Gambhir SS, Chen X. Chapter 7. Molecular imaging of tumor vasculature. Methods Enzymol. 2008; 445:141–176. [PubMed: 19022059]
53. Hiona A, Wu JC. Noninvasive radionuclide imaging of cardiac gene therapy: progress and potential. Nat Clin Pract Cardiovasc Med. 2008; 5(Suppl 2):S87–95. [PubMed: 18641612]
54. Niu G, Chen X. Vascular endothelial growth factor as an anti-angiogenic target for cancer therapy. Curr Drug Targets. 2010; 11:1000–1017. [PubMed: 20426765]
55. Willmann JK, Chen K, Wang H, Paulmurugan R, Rollins M, Cai W, Wang DS, Chen IY, Gheysens O, Rodriguez-Porcel M, Chen X, Gambhir SS. Monitoring of the biological response to murine hindlimb ischemia with ^{64}Cu-labeled vascular endothelial growth factor-121 positron emission tomography. Circulation. 2008; 117:915–922. [PubMed: 18250264]

56. Kang CM, Koo HJ, Lee KC, Choe YS, Choi JY, Lee KH, Kim BT. A vascular endothelial growth factor 121 ($VEGF_{121}$)-based dual PET/optical probe for in vivo imaging of VEGF receptor expression. Biomaterials. 2013; 34:6839–6845. [PubMed: 23787114]
57. Zhang Y, Hong H, Niu G, Valdovinos HF, Orbay H, Nayak TR, Chen X, Barnhart TE, Cai W. Positron Emission Tomography Imaging of Vascular Endothelial Growth Factor Receptor Expression with ^{61}Cu-Labeled Lysine-Tagged $VEGF_{121}$. Mol Pharm. 2012; 9:3586–3594. [PubMed: 23137334]
58. Lu E, Wagner WR, Schellenberger U, Abraham JA, Klibanov AL, Woulfe SR, Csikari MM, Fischer D, Schreiner GF, Brandenburger GH, Villanueva FS. Targeted in vivo labeling of receptors for vascular endothelial growth factor: approach to identification of ischemic tissue. Circulation. 2003; 108:97–103. [PubMed: 12821549]
59. Cai W, Guzman R, Hsu AR, Wang H, Chen K, Sun G, Gera A, Choi R, Bliss T, He L, Li ZB, Maag AL, Hori N, Zhao H, Moseley M, Steinberg GK, Chen X. Positron emission tomography imaging of poststroke angiogenesis. Stroke. 2009; 40:270–277. [PubMed: 18948613]
60. Chan C, Cai Z, Su R, Reilly RM. ^{111}In- or ^{99m}Tc-labeled recombinant VEGF bioconjugates: in vitro evaluation of their cytotoxicity on porcine aortic endothelial cells overexpressing Flt-1 receptors. Nucl Med Biol. 2010; 37:105–115. [PubMed: 20152709]
61. Eder M, Krivoshein AV, Backer M, Backer JM, Haberkorn U, Eisenhut M. ScVEGF-PEG-HBED-CC and scVEGF-PEG-NOTA conjugates: comparison of easy-to-label recombinant proteins for [^{68}Ga]PET imaging of VEGF receptors in angiogenic vasculature. Nucl Med Biol. 2010; 37:405–412. [PubMed: 20447550]
62. Wang H, Gao H, Guo N, Niu G, Ma Y, Kiesewetter DO, Chen X. Site-specific labeling of scVEGF with fluorine-18 for positron emission tomography imaging. Theranostics. 2012; 2:607–617. [PubMed: 22768028]
63. Scheer MG, Stollman TH, Boerman OC, Verrijp K, Sweep FC, Leenders WP, Ruers TJ, Oyen WJ. Imaging liver metastases of colorectal cancer patients with radiolabelled bevacizumab: Lack of correlation with VEGF-A expression. Eur J Cancer. 2008; 44:1835–1840. [PubMed: 18632262]
64. Nayak TK, Garmestani K, Baidoo KE, Milenic DE, Brechbiel MW. PET imaging of tumor angiogenesis in mice with VEGF-A-targeted ^{86}Y-CHX-A″-DTPA-bevacizumab. Int J Cancer. 2011; 128:920–926. [PubMed: 20473899]
65. Paudyal B, Paudyal P, Oriuchi N, Hanaoka H, Tominaga H, Endo K. Positron emission tomography imaging and biodistribution of vascular endothelial growth factor with 64Cu-labeled bevacizumab in colorectal cancer xenografts. Cancer Sci. 2011; 102:117–121. [PubMed: 21070475]
66. Zhang Y, Hong H, Engle JW, Yang Y, Barnhart TE, Cai W. Positron emission tomography and near-Infrared fluorescence imaging of vascular endothelial growth factor with dual-labeled bevacizumab. Am J Nucl Med Mol Imaging. 2012; 2:1–13. [PubMed: 22229128]
67. Chang AJ, Sohn R, Lu ZH, Arbeit JM, Lapi SE. Detection of rapalog-mediated therapeutic response in renal cancer xenografts using ^{64}Cu-bevacizumab immunoPET. PLoS One. 2013; 8:e58949. [PubMed: 23516584]
68. Gaykema SB, Brouwers AH, Lub-de Hooge MN, Pleijhuis RG, Timmer-Bosscha H, Pot L, van Dam GM, van der Meulen SB, de Jong JR, Bart J, de Vries J, Jansen L, de Vries EG, Schroder CP. ^{89}Zr-bevacizumab PET imaging in primary breast cancer. J Nucl Med. 2013; 54:1014–1018. [PubMed: 23651946]
69. Golestani R, Zeebregts CJ, Terwisscha van Scheltinga AG, Lub-de Hooge MN, van Dam GM, Glaudemans AW, Dierckx RATio RA, Suurmeijer AJ, Boersma HH, Nagengast WB, Slart RH. Feasibility of vascular endothelial growth factor imaging in human atherosclerotic plaque using ^{89}Zr-bevacizumab positron emission tomography. Mol Imaging. 2013; 12:235–243. [PubMed: 23651501]
70. Hurwitz H, Fehrenbacher L, Novotny W, Cartwright T, Hainsworth J, Heim W, Berlin J, Baron A, Griffing S, Holmgren E, Ferrara N, Fyfe G, Rogers B, Ross R, Kabbinavar F. Bevacizumab plus irinotecan, fluorouracil, and leucovorin for metastatic colorectal cancer. N Engl J Med. 2004; 350:2335–2342. [PubMed: 15175435]

71. Noguera EC, Palazzo E, Mayoraz MF, Diller A, Burgesser MV, Jaime A, Borello A, Avila R, Mondina JC. Technetium-bevacizumab in a patient with bone and lung metastatic colon adenocarcinoma. J Clin Oncol. 2013; 31:e170–172. [PubMed: 23460717]
72. Stollman TH, Scheer MG, Franssen GM, Verrijp KN, Oyen WJ, Ruers TJ, Leenders WP, Boerman OC. Tumor accumulation of radiolabeled bevacizumab due to targeting of cell- and matrix-associated VEGF-A isoforms. Cancer Biother Radiopharm. 2009; 24:195–200. [PubMed: 19409041]
73. Nagengast WB, Lub-de Hooge MN, Oosting SF, den Dunnen WF, Warnders FJ, Brouwers AH, de Jong JR, Price PM, Hollema H, Hospers GA, Elsinga PH, Hesselink JW, Gietema JA, de Vries EG. VEGF-PET imaging is a noninvasive biomarker showing differential changes in the tumor during sunitinib treatment. Cancer Res. 2011; 71:143–153. [PubMed: 21084271]
74. Samen E, Thorell JO, Lu L, Tegnebratt T, Holmgren L, Stone-Elander S. Synthesis and preclinical evaluation of [^{11}C]PAQ as a PET imaging tracer for VEGFR-2. Eur J Nucl Med Mol Imaging. 2009; 36:1283–1295. [PubMed: 19288096]
75. Ilovich O, Billauer H, Dotan S, Mishani E. Labeled 3-aryl-4-indolylmaleimide derivatives and their potential as angiogenic PET biomarkers. Bioorg Med Chem. 2010; 18:612–620. [PubMed: 20031417]
76. Christoforidis JB, Williams MM, Kothandaraman S, Kumar K, Epitropoulos FJ, Knopp MV. Pharmacokinetic properties of intravitreal I-124-aflibercept in a rabbit model using PET/CT. Curr Eye Res. 2012; 37:1171–1174. [PubMed: 22991959]
77. Ilovich O, Jacobson O, Aviv Y, Litchi A, Chisin R, Mishani E. Formation of fluorine-18 labeled diaryl ureas--labeled VEGFR-2/PDGFR dual inhibitors as molecular imaging agents for angiogenesis. Bioorg Med Chem. 2008; 16:4242–4251. [PubMed: 18343125]
78. Christoforidis JB, Carlton MM, Knopp MV, Hinkle GH. PET/CT imaging of I-124-radiolabeled bevacizumab and ranibizumab after intravitreal injection in a rabbit model. Invest Ophthalmol Vis Sci. 2011; 52:5899–5903. [PubMed: 21685343]
79. Wang H, Cai W, Chen K, Li ZB, Kashefi A, He L, Chen X. A new PET tracer specific for vascular endothelial growth factor receptor 2. Eur J Nucl Med Mol Imaging. 2007; 34:2001–2010. [PubMed: 17694307]
80. Avraamides CJ, Garmy-Susini B, Varner JA. Integrins in angiogenesis and lymphangiogenesis. Nat Rev Cancer. 2008; 8:604–617. [PubMed: 18497750]
81. Danhier F, Le Breton A, Preat V. RGD-based strategies to target alpha(v) beta(3) integrin in cancer therapy and diagnosis. Mol Pharm. 2012; 9:2961–2973. [PubMed: 22967287]
82. Sheldrake HM, Patterson LH. Function and antagonism of beta3 integrins in the development of cancer therapy. Curr Cancer Drug Targets. 2009; 9:519–540. [PubMed: 19519320]
83. Holzmann B, Gosslar U, Bittner M. alpha 4 integrins and tumor metastasis. Curr Top Microbiol Immunol. 1998; 231:125–141. [PubMed: 9479864]
84. Denardo SJ, Liu R, Albrecht H, Natarajan A, Sutcliffe JL, Anderson C, Peng L, Ferdani R, Cherry SR, Lam KS. ^{111}In-LLP2A-DOTA Polyethylene Glycol-Targeting {alpha}4{beta}1 Integrin: Comparative Pharmacokinetics for Imaging and Therapy of Lymphoid Malignancies. J Nucl Med. 2009; 50:625–634. [PubMed: 19289419]
85. Shokeen M, Zheleznyak A, Wilson JM, Jiang M, Liu R, Ferdani R, Lam KS, Schwarz JK, Anderson CJ. Molecular imaging of very late antigen-4 (alpha4beta1 integrin) in the premetastatic niche. J Nucl Med. 2012; 53:779–786. [PubMed: 22496586]
86. Jiang M, Ferdani R, Shokeen M, Anderson CJ. Comparison of two cross-bridged macrocyclic chelators for the evaluation of ^{64}Cu-labeled-LLP2A, a peptidomimetic ligand targeting VLA-4-positive tumors. Nucl Med Biol. 2013; 40:245–251. [PubMed: 23265977]
87. Soodgupta D, Hurchla MA, Jiang M, Zheleznyak A, Weilbaecher KN, Anderson CJ, Tomasson MH, Shokeen M. Very late antigen-4 (alpha(4)beta(1) Integrin) targeted PET imaging of multiple myeloma. PLoS One. 2013; 8:e55841. [PubMed: 23409060]
88. Carman CV. Overview: imaging in the study of integrins. Methods Mol Biol. 2012; 757:159–189. [PubMed: 21909913]
89. Cai W, Niu G, Chen X. Imaging of integrins as biomarkers for tumor angiogenesis. Curr Pharm Des. 2008; 14:2943–2973. [PubMed: 18991712]

90. Liu Z, Wang F. Development of RGD-based radiotracers for tumor imaging and therapy: translating from bench to bedside. Curr Mol Med. 2013; 13:1487–1505. [PubMed: 24206140]
91. Fonsatti E, Sigalotti L, Arslan P, Altomonte M, Maio M. Emerging role of endoglin (CD105) as a marker of angiogenesis with clinical potential in human malignancies. Curr Cancer Drug Targets. 2003; 3:427–432. [PubMed: 14683500]
92. Fonsatti E, Nicolay HJ, Altomonte M, Covre A, Maio M. Targeting cancer vasculature via endoglin/CD105: a novel antibody-based diagnostic and therapeutic strategy in solid tumours. Cardiovasc Res. 2010; 86:12–19. [PubMed: 19812043]
93. Fonsatti E, Maio M. Highlights on endoglin (CD105): from basic findings towards clinical applications in human cancer. J Transl Med. 2004; 2:18. [PubMed: 15193152]
94. Ikushima H, Miyazono K. TGFbeta signalling: a complex web in cancer progression. Nat Rev Cancer. 2010; 10:415–424. [PubMed: 20495575]
95. Dallas NA, Samuel S, Xia L, Fan F, Gray MJ, Lim SJ, Ellis LM. Endoglin (CD105): a marker of tumor vasculature and potential target for therapy. Clin Cancer Res. 2008; 14:1931–1937. [PubMed: 18381930]
96. Rubatt JM, Darcy KM, Hutson A, Bean SM, Havrilesky LJ, Grace LA, Berchuck A, Secord AA. Independent prognostic relevance of microvessel density in advanced epithelial ovarian cancer and associations between CD31, CD105, p53 status, and angiogenic marker expression: A Gynecologic Oncology Group study. Gynecol Oncol. 2009; 112:469–474. [PubMed: 19135712]
97. Fonsatti E, Altomonte M, Nicotra MR, Natali PG, Maio M. Endoglin (CD105): a powerful therapeutic target on tumor-associated angiogenetic blood vessels. Oncogene. 2003; 22:6557–6563. [PubMed: 14528280]
98. Takahashi N, Haba A, Matsuno F, Seon BK. Antiangiogenic therapy of established tumors in human skin/severe combined immunodeficiency mouse chimeras by anti-endoglin (CD105) monoclonal antibodies, and synergy between anti-endoglin antibody and cyclophosphamide. Cancer Res. 2001; 61:7846–7854. [PubMed: 11691802]
99. Lee S, Mandic J, Van Vliet KJ. Chemomechanical mapping of ligand-receptor binding kinetics on cells. Proc Natl Acad Sci U S A. 2007; 104:9609–9614. [PubMed: 17535923]
100. Altomonte M, Montagner R, Fonsatti E, Colizzi F, Cattarossi I, Brasoveanu LI, Nicotra MR, Cattelan A, Natali PG, Maio M. Expression and structural features of endoglin (CD105), a transforming growth factor beta1 and beta3 binding protein, in human melanoma. Br J Cancer. 1996; 74:1586–1591. [PubMed: 8932339]
101. Tabata M, Kondo M, Haruta Y, Seon BK. Antiangiogenic radioimmunotherapy of human solid tumors in SCID mice using ^{125}I-labeled anti-endoglin monoclonal antibodies. Int J Cancer. 1999; 82:737–742. [PubMed: 10417773]
102. Hong H, Yang Y, Zhang Y, Engle JW, Barnhart TE, Nickles RJ, Leigh BR, Cai W. Positron emission tomography imaging of CD105 expression during tumor angiogenesis. Eur J Nucl Med Mol Imaging. 2011; 38:1335–1343. [PubMed: 21373764]
103. Zhang Y, Hong H, Engle JW, Bean J, Yang Y, Leigh BR, Barnhart TE, Cai W. Positron emission tomography imaging of CD105 expression with a ^{64}Cu-labeled monoclonal antibody: NOTA is superior to DOTA. PLoS One. 2011; 6:e28005. [PubMed: 22174762]
104. Bredow S, Lewin M, Hofmann B, Marecos E, Weissleder R. Imaging of tumour neovasculature by targeting the TGF-beta binding receptor endoglin. Eur J Cancer. 2000; 36:675–681. [PubMed: 10738134]
105. Fonsatti E, Jekunen AP, Kairemo KJ, Coral S, Snellman M, Nicotra MR, Natali PG, Altomonte M, Maio M. Endoglin is a suitable target for efficient imaging of solid tumors: in vivo evidence in a canine mammary carcinoma model. Clin Cancer Res. 2000; 6:2037–2043. [PubMed: 10815930]
106. Costello B, Li C, Duff S, Butterworth D, Khan A, Perkins M, Owens S, Al-Mowallad AF, O'Dwyer S, Kumar S. Perfusion of ^{99m}Tc-labeled CD105 Mab into kidneys from patients with renal carcinoma suggests that CD105 is a promising vascular target. Int J Cancer. 2004; 109:436–441. [PubMed: 14961584]
107. Tsujie M, Uneda S, Tsai H, Seon BK. Effective anti-angiogenic therapy of established tumors in mice by naked anti-human endoglin (CD105) antibody: differences in growth rate and

therapeutic response between tumors growing at different sites. Int J Oncol. 2006; 29:1087–1094. [PubMed: 17016638]

108. Rosen LS, Hurwitz HI, Wong MK, Goldman J, Mendelson DS, Figg WD, Spencer S, Adams BJ, Alvarez D, Seon BK, Theuer CP, Leigh BR, Gordon MS. A phase I first-in-human study of TRC105 (anti-endoglin antibody) in patients with advanced cancer. Clin Cancer Res. 2012; 18:4820–4829. [PubMed: 22767667]
109. Zhang Y, Hong H, Engle JW, Yang Y, Theuer CP, Barnhart TE, Cai W. Positron emission tomography and optical imaging of tumor CD105 expression with a dual-labeled monoclonal antibody. Mol Pharm. 2012; 9:645–653. [PubMed: 22292418]
110. Phelps ME, Hoffman EJ, Huang SC, Ter-Pogossian MM. Effect of positron range on spatial resolution. J Nucl Med. 1975; 16:649–652. [PubMed: 1151485]
111. Vosjan MJ, Perk LR, Visser GW, Budde M, Jurek P, Kiefer GE, van Dongen GA. Conjugation and radiolabeling of monoclonal antibodies with zirconium-89 for PET imaging using the bifunctional chelate p-isothiocyanatobenzyl-desferrioxamine. Nat Protoc. 2010; 5:739–743. [PubMed: 20360768]
112. Hong H, Severin GW, Yang Y, Engle JW, Zhang Y, Barnhart TE, Liu G, Leigh BR, Nickles RJ, Cai W. Positron emission tomography imaging of CD105 expression with ^{89}Zr-Df-TRC105. Eur J Nucl Med Mol Imaging. 2012; 39:138–148. [PubMed: 21909753]
113. Zhang Y, Hong H, Severin GW, Engle JW, Yang Y, Goel S, Nathanson AJ, Liu G, Nickles RJ, Leigh BR, Barnhart TE, Cai W. ImmunoPET and near-infrared fluorescence imaging of CD105 expression using a monoclonal antibody dual-labeled with ^{89}Zr and IRDye 800CW. Am J Transl Res. 2012; 4:333–346. [PubMed: 22937210]
114. Hong H, Zhang Y, Severin GW, Yang Y, Engle JW, Niu G, Nickles RJ, Chen X, Leigh BR, Barnhart TE, Cai W. Multimodality Imaging of Breast Cancer Experimental Lung Metastasis with Bioluminescence and a Monoclonal Antibody Dual-Labeled with ^{89}Zr and IRDye 800CW. Mol Pharm. 2012; 9:2339–2349. [PubMed: 22784250]
115. Zhang Y, Hong H, Nayak TR, Valdovinos HF, Myklejord DV, Theuer CP, Barnhart TE, Cai W. Imaging tumor angiogenesis in breast cancer experimental lung metastasis with positron emission tomography, near-infrared fluorescence, and bioluminescence. Angiogenesis. 2013; 16:663–674. [PubMed: 23471463]
116. Wu AM, Olafsen T. Antibodies for molecular imaging of cancer. Cancer J. 2008; 14:191–197. [PubMed: 18536559]
117. Hong H, Zhang Y, Orbay H, Valdovinos HF, Nayak TR, Bean J, Theuer CP, Barnhart TE, Cai W. Positron emission tomography imaging of tumor angiogenesis with a $^{61/64}$Cu-labeled F(ab′)$_2$ antibody fragment. Mol Pharm. 2013; 10:709–716. [PubMed: 23316869]
118. Zhang Y, Hong H, Orbay H, Valdovinos HF, Nayak TR, Theuer CP, Barnhart TE, Cai W. PET imaging of CD105/endoglin expression with a $^{61/64}$Cu-labeled Fab antibody fragment. Eur J Nucl Med Mol Imaging. 2013; 40:759–767. [PubMed: 23344138]
119. Hong H, Zhang Y, Sun J, Cai W. Molecular imaging and therapy of cancer with radiolabeled nanoparticles. Nano Today. 2009; 4:399–413. [PubMed: 20161038]
120. Yang K, Feng L, Hong H, Cai W, Liu Z. Preparation and functionalization of graphene nanocomposites for biomedical applications. Nat Protoc. 2013; 8:2392–2403. [PubMed: 24202553]
121. Hong H, Yang K, Zhang Y, Engle JW, Feng L, Yang Y, Nayak TR, Goel S, Bean J, Theuer CP, Barnhart TE, Liu Z, Cai W. In vivo targeting and imaging of tumor vasculature with radiolabeled, antibody-conjugated nanographene. ACS Nano. 2012; 6:2361–2370. [PubMed: 22339280]
122. Hong H, Zhang Y, Engle JW, Nayak TR, Theuer CP, Nickles RJ, Barnhart TE, Cai W. In vivo targeting and positron emission tomography imaging of tumor vasculature with ^{66}Ga-labeled nano-graphene. Biomaterials. 2012; 33:4147–4156. [PubMed: 22386918]
123. Yang K, Wan J, Zhang S, Tian B, Zhang Y, Liu Z. The influence of surface chemistry and size of nanoscale graphene oxide on photothermal therapy of cancer using ultra-low laser power. Biomaterials. 2012; 33:2206–2214. [PubMed: 22169821]

124. Shi S, Yang K, Hong H, Valdovinos HF, Nayak TR, Zhang Y, Theuer CP, Barnhart TE, Liu Z, Cai W. Tumor vasculature targeting and imaging in living mice with reduced graphene oxide. Biomaterials. 2013; 34:3002–3009. [PubMed: 23374706]

125. Guo J, Hong H, Chen G, Shi S, Zheng Q, Zhang Y, Theuer CP, Barnhart TE, Cai W, Gong S. Image-guided and tumor-targeted drug delivery with radiolabeled unimolecular micelles. Biomaterials. 2013; 34:8323–8332. [PubMed: 23932288]

126. Guo J, Hong H, Chen G, Shi S, Nayak TR, Theuer CP, Barnhart TE, Cai W, Gong S. Theranostic unimolecular micelles based on brush-shaped amphiphilic block copolymers for tumor-targeted drug delivery and positron emission tomography imaging. ACS Appl Mater Interfaces. 2014 Epub.

127. Chen F, Hong H, Zhang Y, Valdovinos HF, Shi S, Kwon GS, Theuer CP, Barnhart TE, Cai W. In vivo tumor targeting, image-guided drug delivery with antibody-conjugated, radiolabeled mesoporous silica nanoparticles. ACS Nano. 2013; 7:9027–9039. [PubMed: 24083623]

128. Zhang Y, Yang Y, Hong H, Cai W. Multimodality molecular imaging of CD105 (Endoglin) expression. Int J Clin Exp Med. 2011; 4:32–42. [PubMed: 21394284]

129. Nissinen L, Kahari VM. Matrix metalloproteinases in inflammation. Biochim Biophys Acta. 2014; 1840:2571–2580. [PubMed: 24631662]

130. Gibson DJ, Schultz GS. Molecular wound assessments: matrix metalloproteinases. Adv Wound Care (New Rochelle). 2013; 2:18–23. [PubMed: 24527319]

131. Khokha R, Murthy A, Weiss A. Metalloproteinases and their natural inhibitors in inflammation and immunity. Nat Rev Immunol. 2013; 13:649–665. [PubMed: 23969736]

132. Matusiak N, van Waarde A, Bischoff R, Oltenfreiter R, van de Wiele C, Dierckx RA, Elsinga PH. Probes for non-invasive matrix metalloproteinase-targeted imaging with PET and SPECT. Curr Pharm Des. 2013; 19:4647–4672. [PubMed: 23339739]

133. Wagner S, Breyholz HJ, Faust A, Holtke C, Levkau B, Schober O, Schafers M, Kopka K. Molecular imaging of matrix metalloproteinases in vivo using small molecule inhibitors for SPECT and PET. Curr Med Chem. 2006; 13:2819–2838. [PubMed: 17073631]

134. Zhang J, Nie L, Razavian M, Ahmed M, Dobrucki LW, Asadi A, Edwards DS, Azure M, Sinusas AJ, Sadeghi MM. Molecular imaging of activated matrix metalloproteinases in vascular remodeling. Circulation. 2008; 118:1953–1960. [PubMed: 18936327]

135. McIntyre JO, Scherer RL, Matrisian LM. Near-infrared optical proteolytic beacons for in vivo imaging of matrix metalloproteinase activity. Methods Mol Biol. 2010; 622:279–304. [PubMed: 20135290]

136. Midwood KS, Hussenet T, Langlois B, Orend G. Advances in tenascin-C biology. Cell Mol Life Sci. 2011; 68:3175–3199. [PubMed: 21818551]

137. Orend G. Potential oncogenic action of tenascin-C in tumorigenesis. Int J Biochem Cell Biol. 2005; 37:1066–1083. [PubMed: 15743679]

138. Schold SC Jr, Zalutsky MR, Coleman RE, Glantz MJ, Friedman AH, Jaszczak RJ, Bigner SH, Bigner DD. Distribution and dosimetry of I-123-labeled monoclonal antibody 81C6 in patients with anaplastic glioma. Invest Radiol. 1993; 28:488–496. [PubMed: 7686539]

139. Akabani G, Reist CJ, Cokgor I, Friedman AH, Friedman HS, Coleman RE, Zhao XG, Bigner DD, Zalutsky MR. Dosimetry of ^{131}I-labeled 81C6 monoclonal antibody administered into surgically created resection cavities in patients with malignant brain tumors. J Nucl Med. 1999; 40:631–638. [PubMed: 10210222]

140. Akabani G, Reardon DA, Coleman RE, Wong TZ, Metzler SD, Bowsher JE, Barboriak DP, Provenzale JM, Greer KL, DeLong D, Friedman HS, Friedman AH, Zhao XG, Pegram CN, McLendon RE, Bigner DD, Zalutsky MR. Dosimetry and radiographic analysis of ^{131}I-labeled anti-tenascin 81C6 murine monoclonal antibody in newly diagnosed patients with malignant gliomas: a phase II study. J Nucl Med. 2005; 46:1042–1051. [PubMed: 15937318]

141. Sampson JH, Akabani G, Friedman AH, Bigner D, Kunwar S, Berger MS, Bankiewicz KS. Comparison of intratumoral bolus injection and convection-enhanced delivery of radiolabeled antitenascin monoclonal antibodies. Neurosurg Focus. 2006; 20:E14. [PubMed: 16709019]

142. Christine C, Koubemba M, Shakir S, Clavier S, Ehret-Sabatier L, Saupe F, Orend G, Charbonniere LJ. Synthesis of an activated phosphonated bifunctional chelate with potential for PET imaging and radiotherapy. Org Biomol Chem. 2012; 10:9183–9190. [PubMed: 23086384]

143. Heuveling DA, de Bree R, Vugts DJ, Huisman MC, Giovannoni L, Hoekstra OS, Leemans CR, Neri D, van Dongen GA. Phase 0 microdosing PET study using the human mini antibody F16SIP in head and neck cancer patients. J Nucl Med. 2013; 54:397–401. [PubMed: 23334725]

144. Aloj L, D'Ambrosio L, Aurilio M, Morisco A, Frigeri F, Caraco C, Di Gennaro F, Capobianco G, Giovannoni L, Menssen HD, Neri D, Pinto A, Lastoria S. Radioimmunotherapy with Tenarad, a ^{131}I-labelled antibody fragment targeting the extra-domain A1 of tenascin-C,in patients with refractory Hodgkin's lymphoma. Eur J Nucl Med Mol Imaging. 2014; 41:867–877. [PubMed: 24435772]

145. Hicke BJ, Stephens AW, Gould T, Chang YF, Lynott CK, Heil J, Borkowski S, Hilger CS, Cook G, Warren S, Schmidt PG. Tumor targeting by an aptamer. J Nucl Med. 2006; 47:668–678. [PubMed: 16595502]

146. Wang AZ, Farokhzad OC. Current progress of aptamer-based molecular imaging. J Nucl Med. 2014; 55:353–356. [PubMed: 24525205]

147. Ko HY, Choi KJ, Lee CH, Kim S. A multimodal nanoparticle-based cancer imaging probe simultaneously targeting nucleolin, integrin alphavbeta3 and tenascin-C proteins. Biomaterials. 2011; 32:1130–1138. [PubMed: 21071077]

148. Boyd AW, Bartlett PF, Lackmann M. Therapeutic targeting of EPH receptors and their ligands. Nat Rev Drug Discov. 2014; 13:39–62. [PubMed: 24378802]

149. Nikolov DB, Xu K, Himanen JP. Eph/ephrin recognition and the role of Eph/ephrin clusters in signaling initiation. Biochim Biophys Acta. 2013; 1834:2160–2165. [PubMed: 23628727]

150. Xi HQ, Wu XS, Wei B, Chen L. Eph receptors and ephrins as targets for cancer therapy. J Cell Mol Med. 2012; 16:2894–2909. [PubMed: 22862837]

151. Lisabeth EM, Falivelli G, Pasquale EB. Eph receptor signaling and ephrins. Cold Spring Harb Perspect Biol. 2013; 5:a009159. [PubMed: 24003208]

152. Cai W, Ebrahimnejad A, Chen K, Cao Q, Li ZB, Tice DA, Chen X. Quantitative radioimmunoPET imaging of EphA2 in tumor-bearing mice. Eur J Nucl Med Mol Imaging. 2007; 34:2024–2036. [PubMed: 17673999]

153. Huang M, Xiong C, Lu W, Zhang R, Zhou M, Huang Q, Weinberg J, Li C. Dual-modality micro-positron emission tomography/computed tomography and near-infrared fluorescence imaging of EphB4 in orthotopic glioblastoma xenograft models. Mol Imaging Biol. 2014; 16:74–84. [PubMed: 23918654]

154. Liu S, Li D, Park R, Liu R, Xia Z, Guo J, Krasnoperov V, Gill PS, Li Z, Shan H, Conti PS. PET imaging of colorectal and breast cancer by targeting EphB4 receptor with ^{64}Cu-labeled hAb47 and hAb131 antibodies. J Nucl Med. 2013; 54:1094–1100. [PubMed: 23667241]

155. Xiong C, Huang M, Zhang R, Song S, Lu W, Flores L 2nd, Gelovani J, Li C. In vivo small-animal PET/CT of EphB4 receptors using ^{64}Cu-labeled peptide. J Nucl Med. 2011; 52:241–248. [PubMed: 21233177]

156. Zhang R, Xiong C, Huang M, Zhou M, Huang Q, Wen X, Liang D, Li C. Peptide-conjugated polymeric micellar nanoparticles for Dual SPECT and optical imaging of EphB4 receptors in prostate cancer xenografts. Biomaterials. 2011; 32:5872–5879. [PubMed: 21612822]

157. Peschard P, Park M. From Tpr-Met to Met, tumorigenesis and tubes. Oncogene. 2007; 26:1276–1285. [PubMed: 17322912]

158. Peruzzi B, Bottaro DP. Targeting the c-Met signaling pathway in cancer. Clin Cancer Res. 2006; 12:3657–3660. [PubMed: 16778093]

159. Lengyel E, Prechtel D, Resau JH, Gauger K, Welk A, Lindemann K, Salanti G, Richter T, Knudsen B, Vande Woude GF, Harbeck N. C-Met overexpression in node-positive breast cancer identifies patients with poor clinical outcome independent of Her2/neu. Int J Cancer. 2005; 113:678–682. [PubMed: 15455388]

160. Petrelli A, Circosta P, Granziero L, Mazzone M, Pisacane A, Fenoglio S, Comoglio PM, Giordano S. Ab-induced ectodomain shedding mediates hepatocyte growth factor receptor down-

regulation and hampers biological activity. Proc Natl Acad Sci U S A. 2006; 103:5090–5095. [PubMed: 16547140]

161. Perk LR, Stigter-van Walsum M, Visser GW, Kloet RW, Vosjan MJ, Leemans CR, Giaccone G, Albano R, Comoglio PM, van Dongen GA. Quantitative PET imaging of Met-expressing human cancer xenografts with 89Zr-labelled monoclonal antibody DN30. Eur J Nucl Med Mol Imaging. 2008; 35:1857–1867. [PubMed: 18491091]
162. Kim EM, Park EH, Cheong SJ, Lee CM, Kim DW, Jeong HJ, Lim ST, Sohn MH, Kim K, Chung J. Characterization, biodistribution and small-animal SPECT of I-125-labeled c-Met binding peptide in mice bearing c-Met receptor tyrosine kinase-positive tumor xenografts. Nucl Med Biol. 2009; 36:371–378. [PubMed: 19423004]
163. Kim EM, Jeong MH, Kim DW, Jeong HJ, Lim ST, Sohn MH. Iodine 125-labeled mesenchymal-epithelial transition factor binding peptide-click-cRGDyk heterodimer for glioma imaging. Cancer Sci. 2011; 102:1516–1521. [PubMed: 21575108]
164. Jagoda EM, Lang L, Bhadrasetty V, Histed S, Williams M, Kramer-Marek G, Mena E, Rosenblum L, Marik J, Tinianow JN, Merchant M, Szajek L, Paik C, Cecchi F, Raffensperger K, Jose-Dizon JM, Bottaro DP, Choyke P. Immuno-PET of the hepatocyte growth factor receptor Met using the 1-armed antibody onartuzumab. J Nucl Med. 2012; 53:1592–1600. [PubMed: 22917884]
165. Vosjan MJ, Vercammen J, Kolkman JA, Stigter-van Walsum M, Revets H, van Dongen GA. Nanobodies targeting the hepatocyte growth factor: potential new drugs for molecular cancer therapy. Mol Cancer Ther. 2012; 11:1017–1025. [PubMed: 22319202]
166. Michaud NR, Jani JP, Hillerman S, Tsaparikos KE, Barbacci-Tobin EG, Knauth E, Putz H Jr, Campbell M, Karam GA, Chrunyk B, Gebhard DF, Green LL, Xu JJ, Dunn MC, Coskran TM, Lapointe JM, Cohen BD, Coleman KG, Bedian V, Vincent P, Kajiji S, Steyn SJ, Borzillo GV, Los G. Biochemical and pharmacological characterization of human c-Met neutralizing monoclonal antibody CE-355621. MAbs. 2012; 4:710–723. [PubMed: 23007574]
167. Wu C, Tang Z, Fan W, Zhu W, Wang C, Somoza E, Owino N, Li R, Ma PC, Wang Y. In vivo positron emission tomography (PET) imaging of mesenchymal-epithelial transition (MET) receptor. J Med Chem. 2010; 53:139–146. [PubMed: 19968287]
168. Martens T, Schmidt NO, Eckerich C, Fillbrandt R, Merchant M, Schwall R, Westphal M, Lamszus K. A novel one-armed anti-c-Met antibody inhibits glioblastoma growth in vivo. Clin Cancer Res. 2006; 12:6144–6152. [PubMed: 17062691]
169. Kosmehl H, Berndt A, Katenkamp D. Molecular variants of fibronectin and laminin: structure, physiological occurrence and histopathological aspects. Virchows Arch. 1996; 429:311–322. [PubMed: 8982375]
170. Midulla M, Verma R, Pignatelli M, Ritter MA, Courtenay-Luck NS, George AJ. Source of oncofetal ED-B-containing fibronectin: implications of production by both tumor and endothelial cells. Cancer Res. 2000; 60:164–169. [PubMed: 10646869]
171. Santimaria M, Moscatelli G, Viale GL, Giovannoni L, Neri G, Viti F, Leprini A, Borsi L, Castellani P, Zardi L, Neri D, Riva P. Immunoscintigraphic detection of the ED-B domain of fibronectin, a marker of angiogenesis, in patients with cancer. Clin Cancer Res. 2003; 9:571–579. [PubMed: 12576420]
172. Carnemolla B, Balza E, Siri A, Zardi L, Nicotra MR, Bigotti A, Natali PG. A tumor-associated fibronectin isoform generated by alternative splicing of messenger RNA precursors. J Cell Biol. 1989; 108:1139–1148. [PubMed: 2646306]
173. Pini A, Viti F, Santucci A, Carnemolla B, Zardi L, Neri P, Neri D. Design and use of a phage display library. Human antibodies with subnanomolar affinity against a marker of angiogenesis eluted from a two-dimensional gel. J Biol Chem. 1998; 273:21769–21776. [PubMed: 9705314]
174. Borsi L, Balza E, Bestagno M, Castellani P, Carnemolla B, Biro A, Leprini A, Sepulveda J, Burrone O, Neri D, Zardi L. Selective targeting of tumoral vasculature: comparison of different formats of an antibody (L19) to the ED-B domain of fibronectin. Int J Cancer. 2002; 102:75–85. [PubMed: 12353237]
175. Tijink BM, Perk LR, Budde M, Stigter-van Walsum M, Visser GW, Kloet RW, Dinkelborg LM, Leemans CR, Neri D, van Dongen GA. ^{124}I-L19-SIP for immuno-PET imaging of tumour

vasculature and guidance of ^{131}I-L19-SIP radioimmunotherapy. Eur J Nucl Med Mol Imaging. 2009; 36:1235–1244. [PubMed: 19259661]

176. Tarli L, Balza E, Viti F, Borsi L, Castellani P, Berndorff D, Dinkelborg L, Neri D, Zardi L. A high-affinity human antibody that targets tumoral blood vessels. Blood. 1999; 94:192–198. [PubMed: 10381513]
177. Sauer S, Erba PA, Petrini M, Menrad A, Giovannoni L, Grana C, Hirsch B, Zardi L, Paganelli G, Mariani G, Neri D, Durkop H, Menssen HD. Expression of the oncofetal ED-B-containing fibronectin isoform in hematologic tumors enables ED-B-targeted ^{131}I-L19SIP radioimmunotherapy in Hodgkin lymphoma patients. Blood. 2009; 113:2265–2274. [PubMed: 19131554]
178. El-Emir E, Dearling JL, Huhalov A, Robson MP, Boxer G, Neri D, van Dongen GA, Trachsel E, Begent RH, Pedley RB. Characterisation and radioimmunotherapy of L19-SIP, an anti-angiogenic antibody against the extra domain B of fibronectin, in colorectal tumour models. Br J Cancer. 2007; 96:1862–1870. [PubMed: 17519905]
179. Berndorff D, Borkowski S, Moosmayer D, Viti F, Muller-Tiemann B, Sieger S, Friebe M, Hilger CS, Zardi L, Neri D, Dinkelborg LM. Imaging of tumor angiogenesis using ^{99m}Tc-labeled human recombinant anti-ED-B fibronectin antibody fragments. J Nucl Med. 2006; 47:1707–1716. [PubMed: 17015908]
180. Rossin R, Berndorff D, Friebe M, Dinkelborg LM, Welch MJ. Small-animal PET of tumor angiogenesis using a ^{76}Br-labeled human recombinant antibody fragment to the ED-B domain of fibronectin. J Nucl Med. 2007; 48:1172–1179. [PubMed: 17574989]
181. Osborn L, Hession C, Tizard R, Vassallo C, Luhowskyj S, Chi-Rosso G, Lobb R. Direct expression cloning of vascular cell adhesion molecule 1, a cytokine-induced endothelial protein that binds to lymphocytes. Cell. 1989; 59:1203–1211. [PubMed: 2688898]
182. Cannistra SA, Ottensmeier C, Tidy J, DeFranzo B. Vascular cell adhesion molecule-1 expressed by peritoneal mesothelium partly mediates the binding of activated human T lymphocytes. Exp Hematol. 1994; 22:996–1002. [PubMed: 7522188]
183. Sans M, Panes J, Ardite E, Elizalde JI, Arce Y, Elena M, Palacin A, Fernandez-Checa JC, Anderson DC, Lobb R, Pique JM. VCAM-1 and ICAM-1 mediate leukocyte-endothelial cell adhesion in rat experimental colitis. Gastroenterology. 1999; 116:874–883. [PubMed: 10092309]
184. Iiyama K, Hajra L, Iiyama M, Li H, DiChiara M, Medoff BD, Cybulsky MI. Patterns of vascular cell adhesion molecule-1 and intercellular adhesion molecule-1 expression in rabbit and mouse atherosclerotic lesions and at sites predisposed to lesion formation. Circ Res. 1999; 85:199–207. [PubMed: 10417402]
185. Chin JE, Hatfield CA, Winterrowd GE, Brashler JR, Vonderfecht SL, Fidler SF, Griffin RL, Kolbasa KP, Krzesicki RF, Sly LM, Staite ND, Richards IM. Airway recruitment of leukocytes in mice is dependent on alpha4-integrins and vascular cell adhesion molecule-1. Am J Physiol. 1997; 272:L219–229. [PubMed: 9124372]
186. Kishimoto H, Sasahara K, Yamazaki K, Nagata T, Uotani H, Yamashita I, Tauchi K, Tsukada K. Obstructive jaundice facilitates hepatic metastasis of B16F1 mouse melanoma cells: participation of increased VCAM-1 expression in the liver. Oncol Rep. 2001; 8:575–578. [PubMed: 11295083]
187. Slack-Davis JK, Atkins KA, Harrer C, Hershey ED, Conaway M. Vascular cell adhesion molecule-1 is a regulator of ovarian cancer peritoneal metastasis. Cancer Res. 2009; 69:1469–1476. [PubMed: 19208843]
188. Scalici JM, Thomas S, Harrer C, Raines TA, Curran J, Atkins KA, Conaway MR, Duska L, Kelly KA, Slack-Davis JK. Imaging vcam-1 as an indicator of treatment efficacy in metastatic ovarian cancer. J Nucl Med. 2013; 54:1883–1889. [PubMed: 24029657]
189. Cao Y. Multifarious functions of PDGFs and PDGFRs in tumor growth and metastasis. Trends Mol Med. 2013; 19:460–473. [PubMed: 23773831]
190. Cryan LM, Rogers MS. Targeting the anthrax receptors, TEM-8 and CMG-2, for anti-angiogenic therapy. Front Biosci (Landmark Ed). 2011; 16:1574–1588. [PubMed: 21196249]
191. Benezra M, Hambardzumyan D, Penate-Medina O, Veach DR, Pillarsetty N, Smith-Jones P, Phillips E, Ozawa T, Zanzonico PB, Longo V, Holland EC, Larson SM, Bradbury MS. Fluorine-

labeled dasatinib nanoformulations as targeted molecular imaging probes in a PDGFB-driven murine glioblastoma model. Neoplasia. 2012; 14:1132–1143. [PubMed: 23308046]

192. Chen KH, Liu S, Bankston LA, Liddington RC, Leppla SH. Selection of anthrax toxin protective antigen variants that discriminate between the cellular receptors TEM8 and CMG2 and achieve targeting of tumor cells. J Biol Chem. 2007; 282:9834–9845. [PubMed: 17251181]
193. Quan Q, Yang M, Gao H, Zhu L, Lin X, Guo N, Zhang G, Eden HS, Niu G, Chen X. Imaging tumor endothelial marker 8 using an ^{18}F-labeled peptide. Eur J Nucl Med Mol Imaging. 2011; 38:1806–1815. [PubMed: 21814853]
194. Yla-Herttuala S. Cardiovascular gene therapy with vascular endothelial growth factors. Gene. 2013; 525:217–219. [PubMed: 23608170]
195. Orbay H, Zhang Y, Hong H, Hacker TA, Valdovinos HF, Zagzebski JA, Theuer CP, Barnhart TE, Cai W. Positron Emission Tomography Imaging of Angiogenesis in a Murine Hindlimb Ischemia Model with ^{64}Cu-Labeled TRC105. Mol Pharm. 2013; 10:2749–2756. [PubMed: 23738915]
196. Orbay H, Hong H, Koch JM, Valdovinos HF, Hacker TA, Theuer CP, Barnhart TE, Cai W. Pravastatin stimulates angiogenesis in a murine hindlimb ischemia model: a positron emission tomography imaging study with ^{64}Cu-NOTA-TRC105. Am J Transl Res. 2013; 6:54–63. [PubMed: 24349621]
197. Orbay H, Zhang Y, Valdovinos HF, Song G, Hernandez R, Theuer CP, Hacker TA, Nickles RJ, Cai W. Positron emission tomography imaging of CD105 expression in a rat myocardial infarction model with ^{64}Cu-NOTA-TRC105. Am J Nucl Med Mol Imaging. 2013; 4:1–9. [PubMed: 24380040]
198. Sato M, Toyozaki T, Odaka K, Uehara T, Arano Y, Hasegawa H, Yoshida K, Imanaka-Yoshida K, Yoshida T, Hiroe M, Tadokoro H, Irie T, Tanada S, Komuro I. Detection of experimental autoimmune myocarditis in rats by 111In monoclonal antibody specific for tenascin-C. Circulation. 2002; 106:1397–1402. [PubMed: 12221059]
199. Kobayashi N, Odaka K, Uehara T, Imanaka-Yoshida K, Kato Y, Oyama H, Tadokoro H, Akizawa H, Tanada S, Hiroe M, Fukumura T, Komuro I, Arano Y, Yoshida T, Irie T. Toward in vivo imaging of heart disease using a radiolabeled single-chain Fv fragment targeting tenascin-C. Anal Chem. 2011; 83:9123–9130. [PubMed: 22074352]
200. Odaka K, Uehara T, Arano Y, Adachi S, Tadokoro H, Yoshida K, Hasegawa H, Imanaka-Yoshida K, Yoshida T, Hiroe M, Irie T, Tanada S, Komuro I. Noninvasive detection of cardiac repair after acute myocardial infarction in rats by ^{111}In Fab fragment of monoclonal antibody specific for tenascin-C. Int Heart J. 2008; 49:481–492. [PubMed: 18753731]
201. Manrique A, Faraggi M, Vera P, Vilain D, Lebtahi R, Cribier A, Le Guludec D. ^{201}Tl and ^{99m}Tc-MIBI gated SPECT in patients with large perfusion defects and left ventricular dysfunction: comparison with equilibrium radionuclide angiography. J Nucl Med. 1999; 40:805–809. [PubMed: 10319754]
202. Orend G, Chiquet-Ehrismann R. Tenascin-C induced signaling in cancer. Cancer Lett. 2006; 244:143–163. [PubMed: 16632194]
203. Barthel SR, Gavino JD, Descheny L, Dimitroff CJ. Targeting selectins and selectin ligands in inflammation and cancer. Expert Opin Ther Targets. 2007; 11:1473–1491. [PubMed: 18028011]
204. Jubeli E, Moine L, Vergnaud-Gauduchon J, Barratt G. E-selectin as a target for drug delivery and molecular imaging. J Control Release. 2012; 158:194–206. [PubMed: 21983284]
205. Keating FK, Dauerman HL, Whitaker DA, Sobel BE, Schneider DJ. Increased expression of platelet P-selectin and formation of platelet-leukocyte aggregates in blood from patients treated with unfractionated heparin plus eptifibatide compared with bivalirudin. Thromb Res. 2006; 118:361–369. [PubMed: 16139336]
206. Xu Y, Li J, Fang W, Yu M, Ru B. A potential thrombus diagnosis reagent based on P-selectin monoclonal antibody SZ-51 light chain. Thromb Res. 2008; 123:306–315. [PubMed: 18692868]
207. Kutlar A, Embury SH. Cellular Adhesion and the Endothelium: P-Selectin. Hematol Oncol Clin North Am. 2014; 28:323–339. [PubMed: 24589269]
208. Rouzet F, Bachelet-Violette L, Alsac JM, Suzuki M, Meulemans A, Louedec L, Petiet A, Jandrot-Perrus M, Chaubet F, Michel JB, Le Guludec D, Letourneur D. Radiolabeled fucoidan as a p-

selectin targeting agent for in vivo imaging of platelet-rich thrombus and endothelial activation. J Nucl Med. 2011; 52:1433–1440. [PubMed: 21849401]

209. Ji S, Fang W, Zhu M, Bai X, Wang C, Ruan C. Detection of pulmonary embolism with 99mTc-labeled F(ab)2 fragment of anti-P-selectin monoclonal antibody in dogs. Tohoku J Exp Med. 2011; 223:9–15. [PubMed: 21187695]
210. Gu J, Liu Y, Xia L, Wan H, Li P, Zhang X, Ruan C. Construction and expression of mouse-human chimeric antibody SZ-51 specific for activated platelet P-selectin. Thromb Haemost. 1997; 77:755–759. [PubMed: 9134655]
211. Li B, Lu F, Wei X, Zhao R. Fucoidan: structure and bioactivity. Molecules. 2008; 13:1671–1695. [PubMed: 18794778]
212. Johnson-Tidey RR, McGregor JL, Taylor PR, Poston RN. Increase in the adhesion molecule P-selectin in endothelium overlying atherosclerotic plaques. Coexpression with intercellular adhesion molecule-1. Am J Pathol. 1994; 144:952–961. [PubMed: 7513951]
213. Bradfield PF, Nourshargh S, Aurrand-Lions M, Imhof BA. JAM family and related proteins in leukocyte migration (Vestweber series). Arterioscler Thromb Vasc Biol. 2007; 27:2104–2112. [PubMed: 17615384]
214. Nakamura I, Hasegawa K, Wada Y, Hirase T, Node K, Watanabe Y. Detection of early stage atherosclerotic plaques using PET and CT fusion imaging targeting P-selectin in low density lipoprotein receptor-deficient mice. Biochem Biophys Res Commun. 2013; 433:47–51. [PubMed: 23485468]
215. Nahrendorf M, Keliher E, Panizzi P, Zhang H, Hembrador S, Figueiredo JL, Aikawa E, Kelly K, Libby P, Weissleder R. ^{18}F-4V for PET-CT imaging of VCAM-1 expression in atherosclerosis. JACC Cardiovasc Imaging. 2009; 2:1213–1222. [PubMed: 19833312]
216. Vosjan MJ, Perk LR, Roovers RC, Visser GW, Stigter-van Walsum M, van Bergen En Henegouwen PM, van Dongen GA. Facile labelling of an anti-epidermal growth factor receptor Nanobody with ^{68}Ga via a novel bifunctional desferal chelate for immuno-PET. Eur J Nucl Med Mol Imaging. 2011; 38:753–763. [PubMed: 21210114]
217. Broisat A, Hernot S, Toczek J, De Vos J, Riou LM, Martin S, Ahmadi M, Thielens N, Wernery U, Caveliers V, Muyldermans S, Lahoutte T, Fagret D, Ghezzi C, Devoogdt N. Nanobodies targeting mouse/human VCAM1 for the nuclear imaging of atherosclerotic lesions. Circ Res. 2012; 110:927–937. [PubMed: 22461363]
218. Broisat A, Riou LM, Ardisson V, Boturyn D, Dumy P, Fagret D, Ghezzi C. Molecular imaging of vascular cell adhesion molecule-1 expression in experimental atherosclerotic plaques with radiolabelled B2702-p. Eur J Nucl Med Mol Imaging. 2007; 34:830–840. [PubMed: 17219135]
219. Dimastromatteo J, Broisat A, Perret P, Ahmadi M, Boturyn D, Dumy P, Fagret D, Riou LM, Ghezzi C. In vivo molecular imaging of atherosclerotic lesions in ApoE−/− mice using VCAM-1-specific, ^{99m}Tc-labeled peptidic sequences. J Nucl Med. 2013; 54:1442–1449. [PubMed: 23719858]
220. Spier BJ, Perlman SB, Reichelderfer M. FDG-PET in inflammatory bowel disease. Q J Nucl Med Mol Imaging. 2009; 53:64–71. [PubMed: 19182729]
221. Kumar V, Boddeti DK. ^{68}Ga-radiopharmaceuticals for PET imaging of infection and inflammation. Recent Results Cancer Res. 2013; 194:189–219. [PubMed: 22918761]
222. Kriegsmann J, Keyszer GM, Geiler T, Lagoo AS, Lagoo-Deenadayalan S, Gay RE, Gay S. Expression of E-selectin messenger RNA and protein in rheumatoid arthritis. Arthritis Rheum. 1995; 38:750–754. [PubMed: 7540009]
223. Jamar F, Houssiau FA, Devogelaer JP, Chapman PT, Haskard DO, Beaujean V, Beckers C, Manicourt DH, Peters AM. Scintigraphy using a technetium ^{99m}Tc-labelled anti-E-selectin Fab fragment in rheumatoid arthritis. Rheumatology (Oxford). 2002; 41:53–61. [PubMed: 11792880]
224. Jamar F, Chapman PT, Manicourt DH, Glass DM, Haskard DO, Peters AM. A comparison between ^{111}In-anti-E-selectin mAb and ^{99m}Tc-labelled human non-specific immunoglobulin in radionuclide imaging of rheumatoid arthritis. Br J Radiol. 1997; 70:473–481. [PubMed: 9227228]
225. Keelan ET, Harrison AA, Chapman PT, Binns RM, Peters AM, Haskard DO. Imaging vascular endothelial activation: an approach using radiolabeled monoclonal antibodies against the

endothelial cell adhesion molecule E-selectin. J Nucl Med. 1994; 35:276–281. [PubMed: 7507524]

226. Garrood T, Blades M, Haskard DO, Mather S, Pitzalis C. A novel model for the pre-clinical imaging of inflamed human synovial vasculature. Rheumatology (Oxford). 2009; 48:926–931. [PubMed: 19491304]
227. Smith DJ, Salmi M, Bono P, Hellman J, Leu T, Jalkanen S. Cloning of vascular adhesion protein 1 reveals a novel multifunctional adhesion molecule. J Exp Med. 1998; 188:17–27. [PubMed: 9653080]
228. Salmi M, Jalkanen S. Cell-surface enzymes in control of leukocyte trafficking. Nat Rev Immunol. 2005; 5:760–771. [PubMed: 16200079]
229. Jalkanen S, Karikoski M, Mercier N, Koskinen K, Henttinen T, Elima K, Salmivirta K, Salmi M. The oxidase activity of vascular adhesion protein-1 (VAP-1) induces endothelial E- and P-selectins and leukocyte binding. Blood. 2007; 110:1864–1870. [PubMed: 17548577]
230. Salmi M, Kalimo K, Jalkanen S. Induction and function of vascular adhesion protein-1 at sites of inflammation. J Exp Med. 1993; 178:2255–2260. [PubMed: 8245796]
231. Salmi M, Jalkanen S. Homing-associated molecules CD73 and VAP-1 as targets to prevent harmful inflammations and cancer spread. FEBS Lett. 2011; 585:1543–1550. [PubMed: 21515268]
232. Lankinen P, Makinen TJ, Poyhonen TA, Virsu P, Salomaki S, Hakanen AJ, Jalkanen S, Aro HT, Roivainen A. ^{68}Ga-DOTAVAP-P1 PET imaging capable of demonstrating the phase of inflammation in healing bones and the progress of infection in osteomyelitic bones. Eur J Nucl Med Mol Imaging. 2008; 35:352–364. [PubMed: 18038133]
233. Ujula T, Salomaki S, Virsu P, Lankinen P, Makinen TJ, Autio A, Yegutkin GG, Knuuti J, Jalkanen S, Roivainen A. Synthesis,^{68}Ga labeling and preliminary evaluation of DOTA peptide binding vascular adhesion protein-1: a potential PET imaging agent for diagnosing osteomyelitis. Nucl Med Biol. 2009; 36:631–641. [PubMed: 19647169]
234. Autio A, Ujula T, Luoto P, Salomaki S, Jalkanen S, Roivainen A. PET imaging of inflammation and adenocarcinoma xenografts using vascular adhesion protein 1 targeting peptide ^{68}Ga-DOTAVAP-P1: comparison with ^{18}F-FDG. Eur J Nucl Med Mol Imaging. 2010; 37:1918–1925. [PubMed: 20523988]
235. Autio A, Henttinen T, Sipila HJ, Jalkanen S, Roivainen A. Mini-PEG spacering of VAP-1-targeting ^{68}Ga-DOTAVAP-P1 peptide improves PET imaging of inflammation. EJNMMI Res. 2011; 1:10. [PubMed: 22214508]
236. Silvola J, Autio A, Luoto P, Jalkanen S, Roivainen A. Preliminary evaluation of novel ^{68}Ga-DOTAVAP-PEG-P2 peptide targeting vascular adhesion protein-1. Clin Physiol Funct Imaging. 2010; 30:75–78. [PubMed: 19840033]
237. Aalto K, Autio A, Kiss EA, Elima K, Nymalm Y, Veres TZ, Marttila-Ichihara F, Elovaara H, Saanijoki T, Crocker PR, Maksimow M, Bligt E, Salminen TA, Salmi M, Roivainen A, Jalkanen S. Siglec-9 is a novel leukocyte ligand for vascular adhesion protein-1 and can be used in PET imaging of inflammation and cancer. Blood. 2011; 118:3725–3733. [PubMed: 21821708]
238. Autio A, Vainio PJ, Suilamo S, Mali A, Vainio J, Saanijoki T, Noponen T, Ahtinen H, Luoto P, Teras M, Jalkanen S, Roivainen A. Preclinical evaluation of a radioiodinated fully human antibody for in vivo imaging of vascular adhesion protein-1-positive vasculature in inflammation. J Nucl Med. 2013; 54:1315–1319. [PubMed: 23847292]
239. Sans M, Fuster D, Vazquez A, Setoain FJ, Piera C, Pique JM, Panes J. ^{123}Iodine-labelled anti-VCAM-1 antibody scintigraphy in the assessment of experimental colitis. Eur J Gastroenterol Hepatol. 2001; 13:31–38. [PubMed: 11204806]
240. Henninger DD, Panes J, Eppihimer M, Russell J, Gerritsen M, Anderson DC, Granger DN. Cytokine-induced VCAM-1 and ICAM-1 expression in different organs of the mouse. J Immunol. 1997; 158:1825–1832. [PubMed: 9029122]
241. Behm CZ, Kaufmann BA, Carr C, Lankford M, Sanders JM, Rose CE, Kaul S, Lindner JR. Molecular imaging of endothelial vascular cell adhesion molecule-1 expression and inflammatory cell recruitment during vasculogenesis and ischemia-mediated arteriogenesis. Circulation. 2008; 117:2902–2911. [PubMed: 18506006]

242. Jung KH, Park BH, Hong SS. Progress in cancer therapy targeting c-Met signaling pathway. Arch Pharm Res. 2012; 35:595–604. [PubMed: 22553051]

243. Menrad A, Menssen HD. ED-B fibronectin as a target for antibody-based cancer treatments. Expert Opin Ther Targets. 2005; 9:491–500. [PubMed: 15948669]

244. O'Connor MK, Li H, Rhodes DJ, Hruska CB, Clancy CB, Vetter RJ. Comparison of radiation exposure and associated radiation-induced cancer risks from mammography and molecular imaging of the breast. Med Phys. 2010; 37:6187–6198. [PubMed: 21302775]

245. Chen K, Chen X. Positron emission tomography imaging of cancer biology: current status and future prospects. Seminars in oncology. 2011; 38:70–86. [PubMed: 21362517]

246. Kang CM, Koo HJ, Choe YS, Choi JY, Lee KH, Kim BT. ^{68}Ga-NODAGA-VEGF$_{121}$ for in vivo imaging of VEGF receptor expression. Nucl Med Biol. 2014; 41:51–57. [PubMed: 24183611]

247. Kettenbach K, Schieferstein H, Ross TL. ^{18}F-labeling using click cycloadditions. BioMed Res Int. 2014; 2014:361329. [PubMed: 25003110]

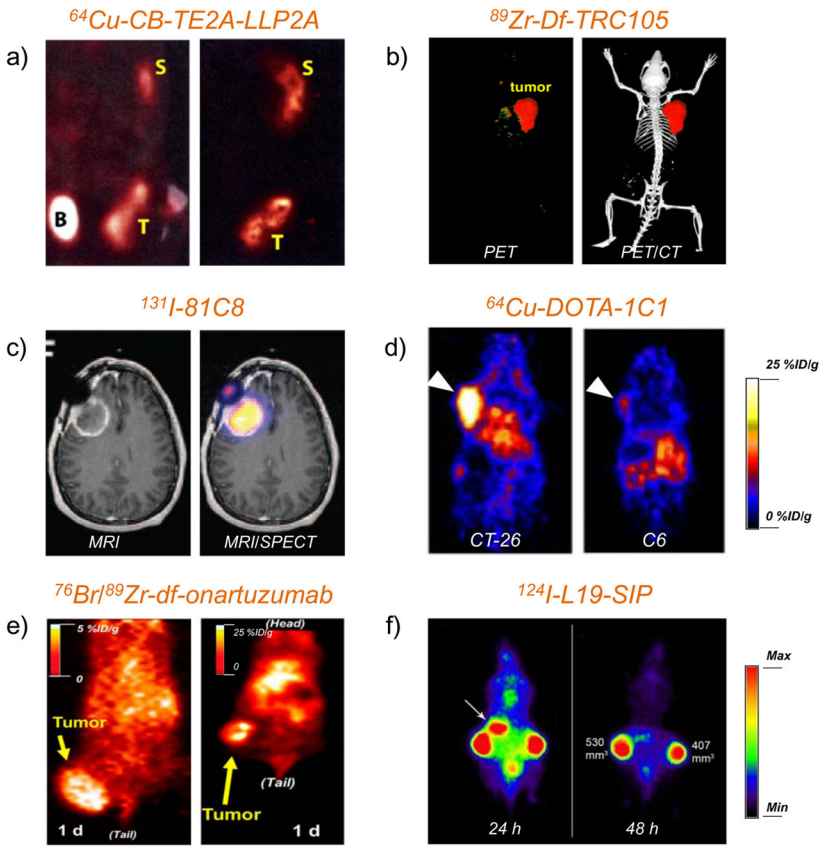

Figure 1. PET or SPECT imaging of vascular targets in cancer models

(**a**) Small-animal PET/CT studies at 4 h p.i. of ^{64}Cu-CB-TE2A-LLP2A in Raji tumor-bearing mice for detection of integrin $\alpha_4\beta_1$ (VLA-4). T: tumor, B: bladder, S: spleen. Adapted with permission from [84]. (**b**) Representative PET/CT images of ^{89}Zr-Df-TRC105 in 4T1 tumor-bearing mice for detection of CD105. Adapted with permission from [112]. (**c**) MRI/SPECT coregistered images of glioma patient injected with ^{131}I-81C8 mAb for detection of tenascin-C positive tumor. Adapted with permission from [140]. Copyright by the Society of Nuclear Medicine and Molecular Imaging, Inc. (**d**) PET images of EphA2 with ^{64}Cu-DOTA-1C1 in mice bearing CT-26 (EphA2-positive) and C6 (EphA2-negative) tumors. Tumors were marked by white arrows. Adapted with permission from [152]. (**e**) Representative coronal PET images of MKN-45 tumor on injected with ^{76}Br-onartuzumab (left) and ^{89}Zr-Df-onartuzumab (right) for imaging of c-Met. Adapted with permission from [164]. Copyright by the Society of Nuclear Medicine and Molecular Imaging, Inc. (**f**) PET images of FaDu xenograft-bearing nude mouse injected with ^{124}I-L19-SIP for detection of ED-B. Uptake in stomach was marked by a white arrow. Adapted with permission from [175].

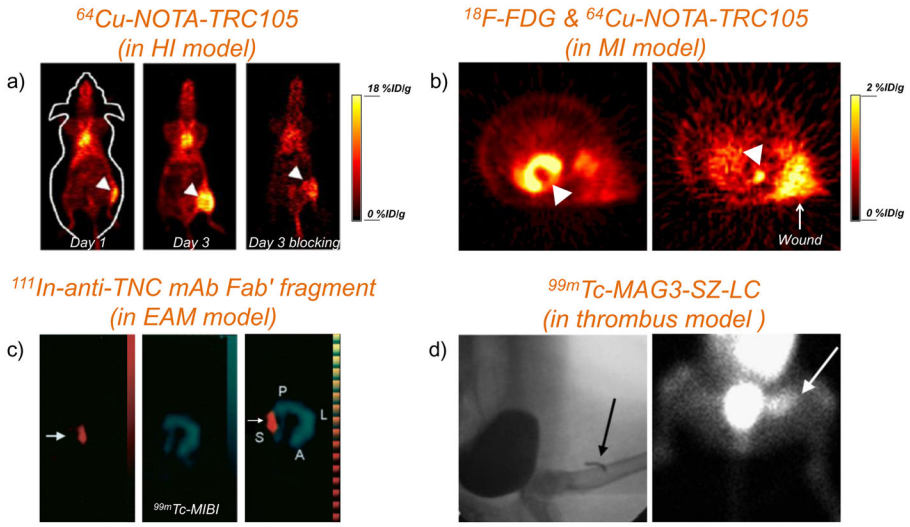

Figure 2. PET or SPECT imaging of vascular targets in cardiovascular disease models

(**a**) Representative PET images at 48 h p.i. of ^{64}Cu-NOTA-TRC105 on day 1 and day 3 after surgical creation of hindlimb ischemia (arrowheads) for detection of CD105. Corresponding PET image of mice in the blocking group on day 3 was also shown. Adapted with permission from [195]. (**b**) PET images with ^{64}Cu-NOTA-TRC105 to detect CD105 expression in a rat myocardial infarction model (pointed by a white arrowhead). Left: PET imaging with ^{18}F-FDG to confirm the presence of myocardial infarction after surgery (pointed by a white arrowhead). Tracer uptake in the wound (pointed by a white arrow) could also be observed. Adapted with permission from [197]. (**c**) SPECT images of ^{111}In-anti-TNC Fab (left panel) and ^{99m}Tc-MIBI (middle panel) in EAM rats. The merged image of these two tracers is shown in the right panel. Adapted with permission from [198]. (**d**) Thrombus imaged with ^{99m}Tc-MAG3-SZ-LC. Arrows indicate the location of copper wire (left, detected by X-ray) and thrombus (right, detected by SPECT). Adapted with permission from [206].

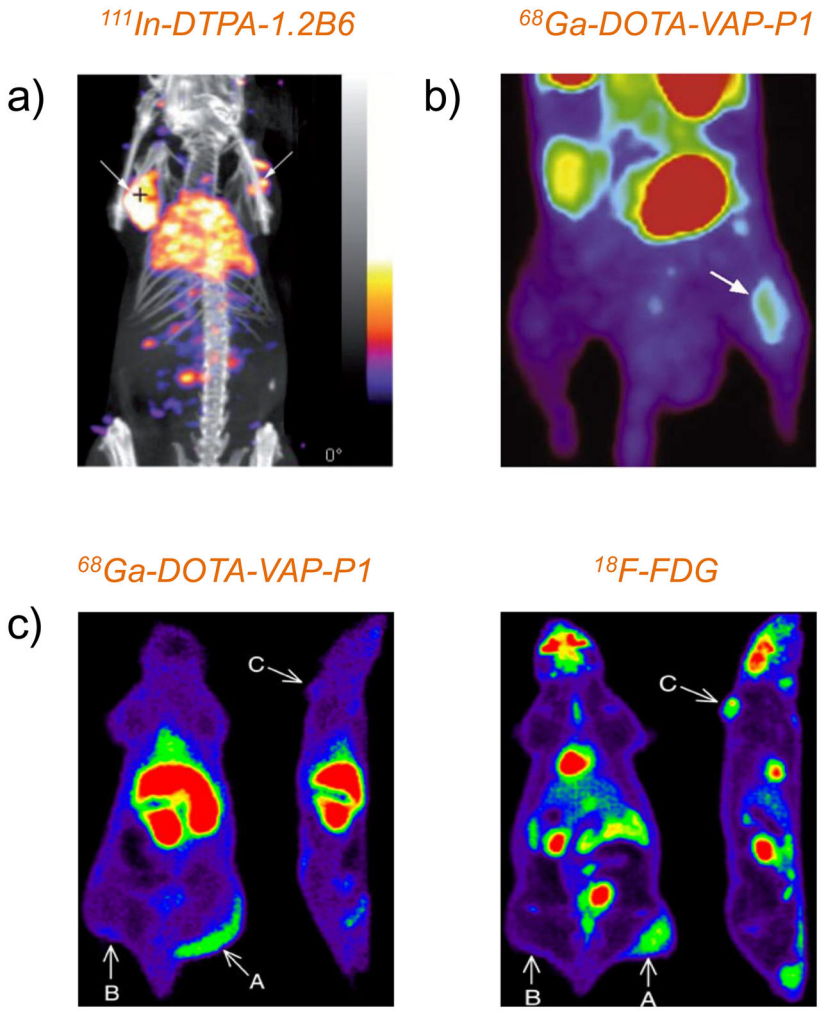

Figure 3. PET or SPECT imaging of vascular targets in inflammation

(**a**) SPECT/CT imaging of a double-transplanted mouse injected with ^{111}In-DTPA-1.2B6 at 5 h post-intragraft injection of TNF-α. White arrows indicated the transplanted synovial tissues. Adapted with permission from [226]. (**b**) Dynamic PET imaging of VAP-1 in osteomyelitic rat after intravenous administration of ^{68}Ga-DOTA-VAP-P1. Clear visualization of the infection focus in the tibia (white arrow) with good target-to-background ratio could be observed. Adapted with permission from [233] (**c**) Representative whole-body coronal and sagittal PET images of a rat intravenously injected with ^{68}Ga-DOTA-VAP-P1 (left) and ^{18}F-FDG (right). Differences in the radioactivity uptake could be clearly seen at the site of inflammation (arrow A), the mouse muscle (arrow B) and the tumor (arrow C), which demonstrated that ^{68}Ga-DOTA-VAP-P1 could discriminate between inflammation and cancer, while ^{18}F-FDG could not. Adapted with permission from [234].

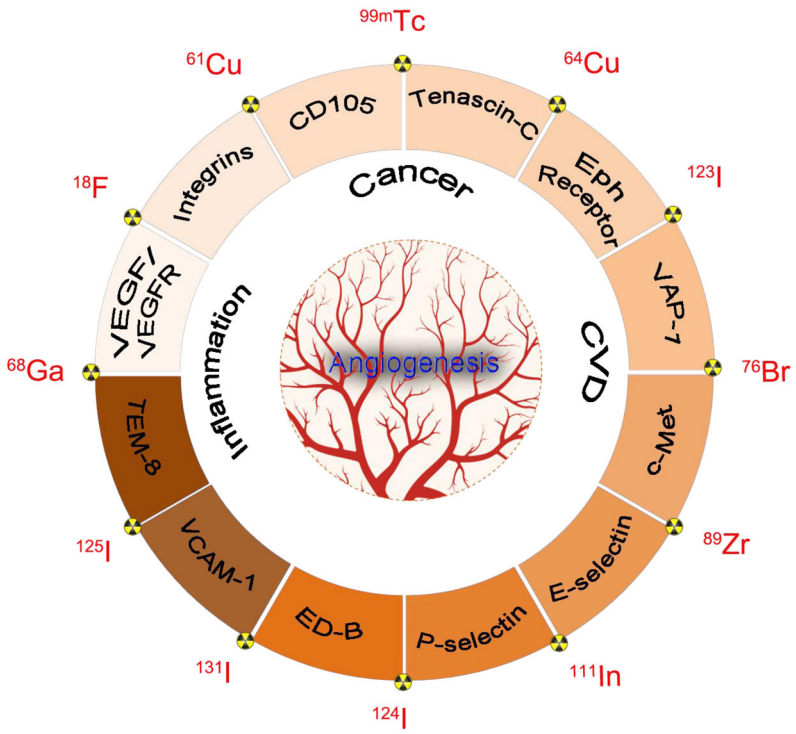

Scheme 1.

A schematic illustration of representative vascular targets and radioisotpes used in PET or SPECT imaging of three major diseases: cancer, cardiovascular diseases (CVD), and inflammation.

Table 1

Representative vascular targets and related PET or SPECT tracers.

Targets	Type of targeting ligands	Representative targeting ligands	Isotopes	Disease models	Stage	Selected References
VEGF	Antibody	Bevacizumab, Ranibizumab	^{111}In, ^{64}Cu, ^{89}Zr	Cancer	Clinical trials	[39, 52]
VEGFR	VEGF isoforms	$VEGF_{121}$, $VEGF_{165}$	$^{61/64}$Cu,^{68}Ga, ^{18}F	Cancer	Preclinical	[39, 52]
	Protein inhibitors	Aflibercept	^{124}I	Eye disease	Clinical trials	[76]
Integrin $\alpha_v\beta_3$	Peptide	RGD	$^{61/64}$Cu,^{68}Ga, ^{18}F	Cancer	Clinical trials	[89, 90]
	Antibody	Abegrin	^{64}Cu	Cancer	Clinical trials	
Integrin $\alpha_4\beta_1$	Peptide	LLP2A	^{64}Cu,^{68}Ga	Cancer	Preclinical	[84, 86]
CD105	Antibody	MAEND3 SN6j TRC105	^{99m}Tc, ^{111}In, ^{64}Cu, ^{89}Zr, ^{64}Cu, ^{66}Ga	Cancer Cardiovascular diseases	Preclinical	[102, 105, 107, 124, 126, 127, 197]
Tenascin-C	Antibody	81C6 B28-13 F16SIP	$^{123/124/131}$I, ^{111}In ^{68}Ga	Cancer Cardiac injury	Clinical trials + preclinical	[140, 143, 200]
Eph receptors	Aptamer	TTA1	^{99m}Tc	Cancer	Preclinical	[145]
	Antibody	1C1 hAb47 hAb131	^{64}Cu	Cancer	Preclinical	[152, 154]
VAP-1	Peptides	TNYL-RAW	^{64}Cu, ^{111}In	Cancer	Preclinical	[153, 155]
	Peptides	VAP-P1 Siglec-9	^{68}Ga	Inflammation	Preclinical	[232, 235–237]
	Antibody	BTT-1023	$^{123/124}$I	Inflammation	Preclinical	[238]
c-Met	Antibody	DN30 Onartuzumab 1E2-Alb8	^{124}I, ^{89}Zr, ^{76}Br	Cancer	Preclinical	[161, 164]
	Peptides	cMBP cMBP-RGD	^{125}I	Cancer	Preclinical	[162, 163]
E-selectin	Antibody	1.2B6	^{125}I, ^{111}In	Inflammation	Clinical trials +Preclinical	[223, 224]

Targets	Type of targeting ligands	Representative targeting ligands	Isotopes	Disease models	Stage	Selected References
P-selectin	Antibody and fragments	SZ-LC SZ51-F(ab)$_2$ RB40.34	^{64}Cu, ^{99m}Tc	Inflammation, Atherosclerosis	Preclinical	[206, 209, 214]
		Fucoidan	^{99m}Tc	Thrombus, Myocardial ischemia	Preclinical	[208]
ED-B	Antibody fragments	L19-SIP	$^{123/124125//131}$I, ^{99m}Tc, ^{76}Br	cancer	Clinical trials + preclinical	[175]
VCAM-1	Antibody Nanobody	4V	^{18}F, ^{99m}Tc	Atherosclerosis	Preclinical	[215]
	Peptides	B2702-p and B2702-rp	^{99m}Tc, ^{123}I	Inflammation	Preclinical	[218, 219]
TEM-8	Peptides	13-meric peptide	^{18}F	Cancer	Preclinical	[193]